Journal of Materials Processing Tech. 319 (2023) 118055

Contents lists available at ScienceDirect

Journal of Materials Processing Tech.

journal homepage: www.elsevier.com/locate/jmatprotec

Quantification of the influence of anisotropic plastic yielding on cold rolling force

L.J.M. Jacobs [a,b,*], E.H. Atzema [b], J. Moerman [b], M.B. de Rooij [a]

[a] Chair of Surface Technology & Tribology, Department of Mechanics of Solids, Surfaces & Systems (MS3), Faculty of Engineering Technology, University of Twente, 7500 AE Enschede, the Netherlands
[b] Tata Steel, Research & Development, 1951 JZ Velsen-Noord, the Netherlands

ARTICLE INFO

Associate Editor: Zhenshan Cui

Keywords:
Cold Rolling
Low-Carbon Steel
Anisotropic Yielding Behaviour
Lankford Parameter
Rolling Models

ABSTRACT

Anisotropic mechanical properties in sheet material are of high importance, in particular for material to be used in stamping or deep drawing applications. The cold rolling process has a marked influence on the degree of anisotropy in the final product. However, the influence of material anisotropy on the cold rolling process itself has so far not been rigorously investigated.

In this work, the degree of normal anisotropy is determined for two low-carbon steel grades after various degree of cold rolling reduction, both by X-ray diffraction as well as by tensile testing. The experimental work shows that material with high cold rolling reduction has non-negligible anisotropic properties; as a consequence the rolling force is seriously overestimated by cold rolling models with an isotropic yield criterion. It is therefore proposed to use the Hill48 yield criterion (instead of the von Mises criterion) in cold rolling models, this criterion takes anisotropic material behaviour into account. A comparison of cold rolling experiments with model predictions confirms that including the Hill48 yield criterion significantly improves the accuracy of a cold rolling model.

1. Introduction

Cold rolling is a process in which material is fed through a set of work rolls. By exerting force on these work rolls the thickness of sheet material is reduced. Due to the high speed and semi-continuous operation, the rolling process is the most widely used process in industry to reduce the thickness of steel sheet. Industrial interest has led researchers to develop models that are used by operators, researchers and scientists to better predict, analyse and understand the rolling process. Montmitonnet (2006) gives a good overview of the state of the art for cold rolling models.

The predictive value of a cold rolling model depends, besides on an accurate description of friction and work roll flattening, largely on the description of plastic yielding behaviour of the material in the roll bite (Yuen et al., 1996a). Various models are available that quantify the work hardening of low-carbon steel; the most widely used are empirical models such as Swift's law (Swift, 1952) or Ludwik's law (Ludwik, 1909) as well as physically based models describing dislocation density such as the model by Bergstrom (1969) that was later improved by van Liempt (1994). All these work hardening models consist of fit parameters that must be obtained by material characterisation. Because cold rolling is primarily a plane strain deformation process, a logical experiment to determine these properties is the plane strain compression test (PSCT) as the stress state is similar. Indeed Pietrzyk et al. (1993) conclude that the PSCT is a predictive experiment for the flat rolling processes, as long as the shape factor is equal. However, Silk and van der Winden (1999) also indicate some disadvantages of this method: the influence of friction cannot be neglected and also bulging of the test sample must be accounted for. Aksenov et al. (2015) further remark that the temperature and strain rate distribution are not uniform over the test sample, i.e. shear bands are formed. All these effects should be taken into account, otherwise the results of the PSCT might not deliver the desired accuracy. Other plane strain tests have been designed that avoid the aforementioned disadvantages of the PSCT, for example An et al. (2004) used a plane strain tensile test. However, this method cannot conveniently be used on full-hard material.

A completely different approach to quantify the material behaviour during cold rolling is by back-calculation from process data. In this case, the yield stress in a cold rolling model is varied until its results (e.g.

* Corresponding author at: Chair of Surface Technology & Tribology, Department of Mechanics of Solids, Surfaces & Systems (MS3), Faculty of Engineering Technology, University of Twente, 7500 AE Enschede, the Netherlands.
E-mail address: l.j.m.jacobs@utwente.nl (L.J.M. Jacobs).

https://doi.org/10.1016/j.jmatprotec.2023.118055
Received 17 February 2023; Received in revised form 16 May 2023; Accepted 5 June 2023
Available online 8 June 2023

Nomenclature

E_{roll}	Youngs modulus of work roll material
P	Work roll force
PS	Plane strain factor, defined as: $PS = \sigma_{PS,yield}/\sigma_{UN,yield}$
r_0, r'	Original work roll radius and Hitchcock work roll radius
R	Lankford parameter for planar isotropic material
R_α	Lankford parameter in direction with angle α to the rolling direction
t	Strip thickness
w	Strip width
ε_x, ε_y, ε_z	Strain in rolling direction, transversal direction and thickness direction
ε_{equiv}	Equivalent strain
θ	Local angle of the tangent to the work roll and the horizontal
μ	Coulomb coefficient of friction
ν_{roll}	Poisson ratio of work roll material
σ_x, σ_y, σ_z	Stress in rolling direction, transversal direction and thickness direction
σ_{yield}	Von Mises yield stress
$\sigma_{PS,yield}$	Yield stress in plane strain point
$\sigma_{UN,yield}$	Yield stress in uniaxial tensile test
τ	Shear stress

rolling force) correspond to measured data. The disadvantage of this method is that the frictional behaviour during cold rolling is also input in the model and must be quantitatively understood. Boemer (2020) gives a complete overview of the state of the art in this field, but it must be concluded that even the most accurately mixed-lubrication models are not accurate enough. Both Pires et al. (2009) and Fouratier et al. (2002) apply a roll force adaptation by simultaneously fitting both friction and yield stress. Although this results in a good prediction of rolling force, most likely it does not result in an accurate description of material behaviour and friction in the roll bite as the underlying physical phenomena are not captured accurately enough.

A final, most commonly used, option to determine the material behaviour in the roll bite is to use the uniaxial tensile test. It allows measuring the yield stress and does not suffer from the drawbacks mentioned for tests with plane strain geometry. However, for a cold rolling model the uniaxial yield point must be translated to the plane strain yield point. This can be achieved by employing a yield criterion, quantifying yielding conditions for a triaxial stress state. Two yield criteria are widely used: the criterion by Tresca (1864) is mathematically simple, but for cold rolling of steel the criterion by von Mises (1913) is found to be more accurate (Lucci et al., 2020). However, both criteria assume that the material behaviour is isotropic which might not be true considering the directionality that is introduced by cold rolling. This work describes the degree of anisotropy of two low-carbon steel grades and the influence of this anisotropy on the predicted cold rolling force.

The degree of anisotropy can be measured in a standard tensile test, Lankford et al. (1950) expressed it by the Lankford parameter R:

$$R_\alpha = \frac{\varepsilon_y}{\varepsilon_z} = \frac{\varepsilon_y}{-\varepsilon_x - \varepsilon_y} \tag{1}$$

Where ε_y and ε_z are respectively the plastic strain in transversal and thickness direction and α is the angle of the tensile sample with the rolling direction. The second equality sign is valid because the total plastic strain is zero, the consequence of volume conservation.

When $R_\alpha \neq 1$ the material is said to be normal anisotropic, while $R_\alpha = 1$ for normal isotropic material. If the Lankford parameter does not depend on the angle with the rolling direction the material is said to be planar isotropic, while for planar anisotropic material the Lankford parameter does depend on α.

Experimentally it is easier to determine the strain in rolling and transversal direction than the strain in thickness direction, therefore the Lankford parameter is determined by measuring ε_y and ε_x. The option to measure these strains is available in many modern tensile testers. However, a complicating factor is that the uniform elongation on cold rolled material is extremely low, therefore the expected strains are very small and material can break outside the uniform area. Therefore, in this work the Lankford parameter has also been determined by a Digital Image Correlation (DIC) method, as described for example by Abspoel (2022).

In the sheet metal forming industry it is well-known that material behaviour is normally not isotropic which is often even desirable: a high Lankford coefficient results in good deep-drawability (Lankford et al., 1950). Therefore the use of anisotropic yield criteria in forming models is absolutely necessary to correctly describe material flow. The Hill48 criterion (Hill, 1948) is, like the von Mises criterion, a quadratic yield criterion that enables to describe normal anisotropy only with a small set of parameters. Vegter et al. (1995) and Vegter and van den Boogaard (2006) present non-quadratic yield functions, the former for planar isotropic material and the latter for planar anisotropic material. Both describe a yield criterion based on experimental results of 4 different mechanical tests, the yield locus is obtained by interpolating between these results using Bézier functions. Other models have been widely used as well, Marzia (2020) provides an overview of the state of the art in this field.

As mentioned before, in analytic cold rolling models always isotropic yield criteria are used. However, this is a questionable assumption because cold rolling results in highly deformed and elongated grains in the rolling direction. This is accompanied by lattice rotation, most likely leading to a significant normal anisotropy. Many researchers have investigated the crystallographic texture of cold rolled steel, usually with the objective to correlate texture with final product properties. Dorner et al. (2006) analyse the magnetic properties of grain-oriented electrical steel, Engler et al. (2000) investigate the influence of texture on formability and Renavikar et al. (2002) describe the influence of texture on springback during forming operations. Modelling of texture is therefore also very important, as in Wang et al. (2021).

Moerman (2005) has already shown that non-uniform crystallographic texture should have an influence on the rolling force during cold rolling. This is further specified in this work: next to measuring the normal anisotropy on a tensile tester with a DIC-method, the influence on the rolling force prediction is also described in more detail. A further novelty of this work is that, by means of an experimental validation, it is shown that it is not accurate enough to use the isotropic von Mises criterion in cold rolling models. Finally it is demonstrated that using the Hill48 yield criterion in a cold rolling model results in better agreement between experimental data and model simulations.

2. Theoretical background

This section describes the theory that is used to analyse the experimental results. Both the constitutive behaviour of the material is detailed as well as the cold rolling model that is used to interpret the results from the rolling trials.

2.1. Yield criteria

Normally in cold rolling models for low-carbon steel, the von Mises yield criterion is used to translate the yield stress from the uniaxial tensile test to a yielding condition in plane strain condition. This yield criterion can be expressed as:

$$\sigma_{yield} = \frac{1}{\sqrt{2}}\sqrt{(\sigma_x-\sigma_y)^2+(\sigma_y-\sigma_z)^2+(\sigma_z-\sigma_x)^2+6(\tau_{xy}^2+\tau_{yz}^2+\tau_{zx}^2)} \quad (2)$$

For some other materials the Tresca yield criterion is considered more suitable:

$$\sigma_{yield} = \max\{|\sigma_x-\sigma_y|;|\sigma_y-\sigma_z|;|\sigma_z-\sigma_x|\} \quad (3)$$

In both equations, σ_{yield} is the yield stress obtained from the tensile test and σ_i and τ_{ij} are the stress components in the Cauchy stress tensor. Both the Tresca criterion as well as the von Mises criterion describe isotropic material behaviour.

In cold rolling models it is common to assume that the rolling direction, normal direction and transversal direction are directions of principal stress, then the von Mises criterion can be simplified to:

$$\sigma_{yield} = \frac{1}{\sqrt{2}}\sqrt{(\sigma_x-\sigma_y)^2+(\sigma_y-\sigma_z)^2+(\sigma_z-\sigma_x)^2} \quad (4)$$

The flow rule expresses that the strain increment has the same direction as the deviatoric stress. This provides another relation between σ_x, σ_y and σ_z, which allows to write Eq. 4 in the following convenient form:

$$\sigma_z = \sigma_x - \frac{2}{\sqrt{3}}\sigma_{yield} \quad (5)$$

This expression is commonly used in slab method cold rolling models (Montmitonnet, 2006).

Anisotropy has a significant influence on the position of the yield locus; the Hill48 criterion allows to take both normal and planar anisotropy into account. In the most general form it can be expressed as (Hill, 1948):

$$\sigma_{yield} = \frac{1}{\sqrt{2}}\sqrt{F(\sigma_x-\sigma_y)^2+G(\sigma_y-\sigma_z)^2+H(\sigma_z-\sigma_x)^2+2L\tau_{xy}^2+2M\tau_{yz}^2+2N\tau_{zx}^2} \quad (6)$$

In this equation F, G, H, L, M and N are constants that still have to be determined experimentally. Van den Boogaard (2002) shows that for normally anisotropic but planar isotropic material the Hill48 criterion can be simplified to:

$$R(\sigma_x-\sigma_y)^2+(\sigma_y-\sigma_z)^2+(\sigma_z-\sigma_x)^2 = (R+1)\sigma_{yield}^2 \quad (7)$$

Where R is the Lankford parameter, which is independent of direction because of the assumed planar isotropy. Cold rolled material is not planar isotropic material, but since cold rolling is primarily a plane strain process, Eq. 7 can be used with the Lankford parameter determined in the rolling direction, i.e. R_0. The difference between the Tresca criterion, the von Mises criterion and the Hill48 criterion (for two different values of R_0) is shown in Fig. 1a. This graph shows the relevance of determining the Lankford parameter for cold rolled material (after different stages of deformation). Based on the Hill48 criterion, the plane strain condition reads (van den Boogaard, 2002):

$$\sigma_z = \sigma_x - \frac{\sigma_{PS,yield}}{\sigma_{UN,yield}}\sigma_{UN,yield} = \sigma_x - \frac{R_0+1}{\sqrt{2R_0+1}}\sigma_{UN,yield} \quad (8)$$

Where $\sigma_{PS,yield}$ and $\sigma_{UN,yield}$ are respectively the plane strain yield point and uniaxial yield point. Obviously, for $R_0 = 1$, the commonly used plane strain condition is found that results from the isotropic von Mises criterion (Eq. 5). According to Eq. 8, the R_0-value significantly influences the vertical stresses in the roll bite. To quantify this, the plane strain factor PS is defined as the ratio between the yield point in plane strain and the uniaxial yield point:

$$PS = \frac{\sigma_{PS,yield}}{\sigma_{UN,yield}} = \frac{R_0+1}{\sqrt{2R_0+1}} \quad (9)$$

Fig. 1b shows the plane strain factor as a function of the Lankford parameter. For R_0-values different from 1 the plane strain factor can significantly deviate from $2/\sqrt{3}$, which has a significant influence on the calculation of vertical pressure in the roll bite and hence on the rolling force.

In cold rolling, on the yield locus only the position of the plane strain yield point is relevant. Because the plane strain yield point is relatively close to the uniaxial yield point, it can be accurately determined from the uniaxial yield point. It will be shown in this work that due to cold rolling, R_0 decreases below 1. Fig. 2 shows experimental results from Abspoel et al. (2017) for a variety of different materials, proving that for $R_0 < 1$ the Hill48 criterion accurately predicts the plane strain yield point. Therefore, in this work the Hill48 criterion has been used to quantify the influence of anisotropy on the plane strain factor.

2.2. Cold rolling model

Montmitonnet (2006) provides an overview of the available types of cold rolling models. The so called slab-model is the most widely used model to describe the cold rolling process. The basis of this model is the von Karman equation (Von Karman, 1925), describing force equilibrium in the vertical slabs of the material (see for example Montmitonnet, 2006):

$$\frac{\partial(t\,\sigma_x)}{\partial x} = 2\sigma_z\frac{\tan(\theta)\pm\mu}{1\mp\mu\tan(\theta)} \quad (10)$$

where t is the strip thickness, σ_z and σ_x respectively the stress in normal

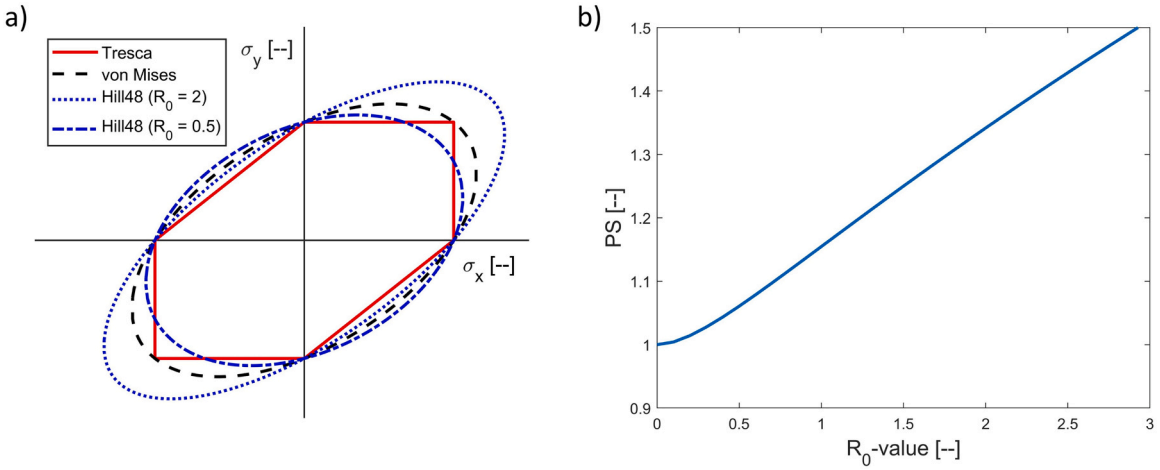

Fig. 1. a) Yield locus in σ_x, σ_y-plane. b) plane strain factor as a function of the Lankford parameter (according to the Hill48 yield criterion).

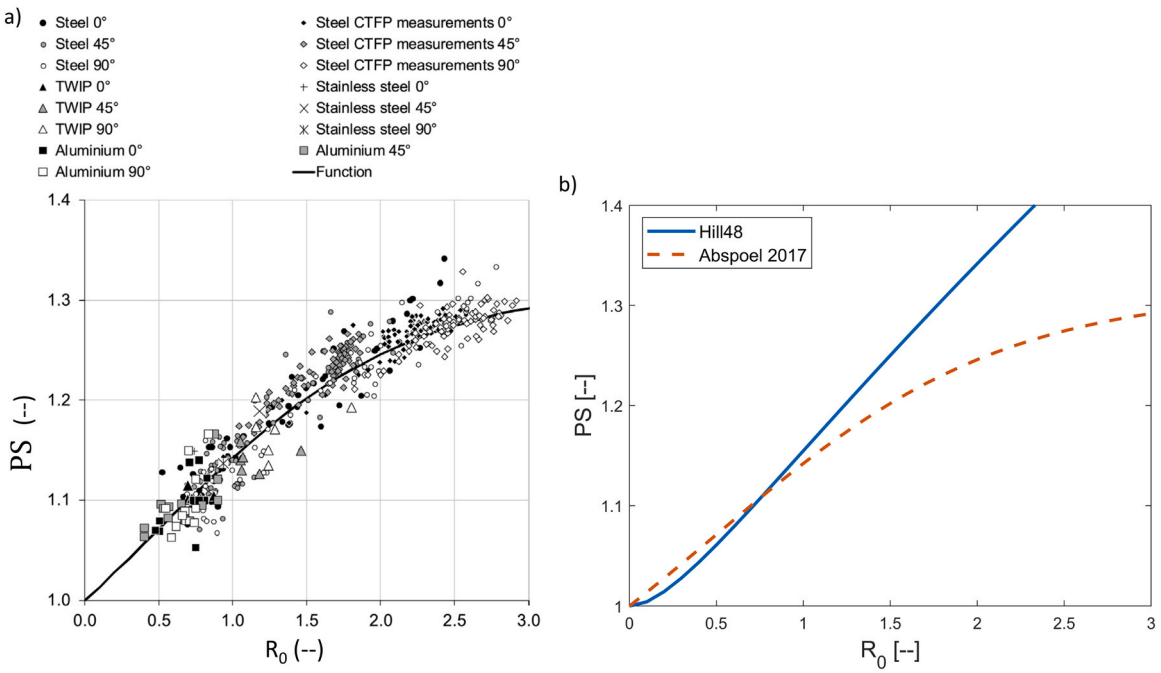

Fig. 2. a) Experimental results reproduced from Abspoel et al. (2017). b) comparison of plane strain factor from Abspoel et al. (2017) with prediction by Hill48 criterion.

direction and rolling direction, μ the coefficient of friction and θ the local angle of the tangent to the work roll and the horizontal. The top signs in Eq. 10 are valid before the neutral point, while the bottom signs are valid after the neutral point. In this work, for reasons of simplicity, material behaviour is considered to be purely plastic (elastic recovery zone is not modelled). Using Eq. 8 allows to write this equation only in term of σ_x, μ and material properties:

$$\frac{\partial(t\sigma_x)}{\partial x} = -2(\sigma_x - \frac{R_0+1}{\sqrt{2R_0+1}}\sigma_{flow})\frac{\tan(\theta)\pm\mu}{1\mp\mu\tan(\theta)} \tag{11}$$

In the model, the Bergstrom-van Liempt model (van Liempt, 1994) is used to describe the work hardening behaviour of low-carbon steel. Viscoplastic behaviour is taken into account as described in Krabiell and Dahl (1981).

Friction between strip and work roll is described in the model by Coulombs law:

$$\tau_{xy} \leq \mu p \tag{12}$$

where normally the equality sign is used because slipping friction is assumed. It is well-known that a higher coefficient of friction results in higher vertical pressure in the roll gap and consequently higher rolling loads. More accurate descriptions of friction in the roll bite are available, Boemer (2020) provides an overview of the state of the art in Mixed-Lubrication modelling. For the current work the rolling model is mainly used to calculate a lower bound for the rolling force, which is achieved by extrapolating the rolling force with the model for $\mu \to 0$. Therefore in this work the Coulomb friction law can be conveniently used.

Another crucial part of the cold rolling model is a description of the elastic work roll flattening. Usually the contact geometry in cold rolling is assumed to be circular, but with a local radius given by Hitchcock (1935):

$$r' = r_0(1 + \frac{16(1-\nu_{roll}^2)}{\pi E_{roll}}\frac{P}{w(t_{in}-t_{out})}) \tag{13}$$

Where r_0 is the original work roll radius, P is the rolling load, w the strip width, E_{roll} the Young's modulus and ν_{roll} the Poisson ratio.

In the model, strip heating is considered to be adiabatic. Heat generated due to plastic deformation distributes uniformly over the strip thickness and heat generated due to friction distributes evenly over strip/roll surface.

The total rolling model consists of an inner-loop and outer-loop. The inner loop finds the neutral point position so that entry/exit tension correspond with the input. The outer-loop assures that the strip thickness profile in the contact corresponds both with the von Karman equation as well as the elastic work roll flattening. Further details can be found in Montmitonnet (2006).

As mentioned in the introduction, both the description of frictional behaviour as well as material behaviour are the main uncertain factors in this model. Other parts of the model are validated for the rolling processes considered in this work or have relatively little influence on the rolling force:

- According to Montmitonnet (2006), using the slab method is allowed when roll-strip contact length is greater than 3 times the entry thickness.
- According to Shigaki et al. (2015), roll flattening is accurately described by Eq. 13 as long as $r' \leq 2 \bullet r_0$. For these conditions Jacobs et al. (2022) have also experimentally validated Eq. 13 with measurements of the contact geometry.
- The thermal part of the model is a simplification of reality. However, according to the Bergstrom-van Liempt model (van Liempt, 1994), the strip temperature only has a limited influence on the work hardening behaviour and the rolling force.
- Including an elastic recovery zone usually increases the rolling force prediction by the model. Here, the prime interest is to find a lower bound for the rolling force; neglecting elastic deformation of the strip gives a good approximation of this value.

Therefore, if friction could be eliminated, the material behaviour could be back-calculated from the experimental results. Obviously, eliminating friction is purely hypothetical; rolling would only be possible for specific combinations of entry and exit tension: the exit tension would have to be much higher than the entry tension to draw the material in the roll bite. To approach the no-friction condition, in the

experiments the friction is decreased as much as experimentally possible. The model is then used to calculate a lower bound for the rolling force by using $\mu = 0$. More precisely: because the model does not converge for $\mu = 0$, the lower bound is obtained by extrapolation.

3. Experimental method

3.1. Tensile tests

Tensile tests were carried out on a Zwick/Roell Z250 tester. The strain rate during the experiments is kept constant during each trial, at $2.5{\cdot}10^{-4}$ s^{-1} for the samples that were 10 % cold rolled or less and at $6.3{\cdot}10^{-5}$ s^{-1} for the samples with more than 10 % cold reduction.

The sample width is measured during testing via a light system at 5–9 different locations over the length of the tensile sample, enabling an accurate estimation of the strain in width direction, even when some inhomogeneity is present. Together with the measured strain in length direction, the R_0-value can be calculated. Furthermore, an ARAMIS Digital Image Correlation (DIC) system is used to independently measure the strain in width and length direction over an area, enabling an even more accurate determination of the R_0-value. To provide the necessary contrast for DIC, the tensile samples were painted white and then sprayed with graphite powder, a photo of an in-situ sample is shown in Fig. 3a. A reference point is chosen manually (also shown in Fig. 3a); the DIC analysis is performed over an area in width and in longitudinal direction from −40 mm to +40 mm relative to this reference point, this area increases during the test with the nominal longitudinal strain. During the tensile test, typically 1 photo per second is taken and the strain in transversal and longitudinal direction is calculated from these DIC-images, an example of the calculated strain distribution is shown in Fig. 3b. At each time step, ε_x and ε_y are averaged over the area of analysis. The evolution of these averages during the test is shown in Fig. 3c. The R-value is calculated with Eq. 1 using strain increments related to the onset of plastic deformation. Fig. 3d shows the calculated R_0-value as function of the longitudinal strain. R_0 is taken as the average calculated R-value over a longitudinal strain range of 1–1.5 %, this range was chosen to avoid any yield point phenomena or elastic effects.

3.2. Texture measurement

A commonly used technology to measure the crystallographic texture is X-ray diffraction (see for example Schwarzer (1991) for a concise description of the experimental method or Bunge (1993) for a detailed overview of textural analysis). The as-rolled samples were ground to half-thickness and a mirror polish was applied. The samples were etched for 15 min in a solution of phosphoric acid, hydrogen peroxide, ethylene glycol monobutyl ether and demineralized water. After rinsing with water, XRD was performed on a fully automated Bruker D8 diffractometer equipped with a 2D area detector. Secondary Kα radiation from a Cobalt tube was used with a characteristic wavelength of 1.79 Å. Per sample, an area of $10{\times}10mm^2$ was scanned in reflection mode using a 3 mm diameter beam formed by a collimator.

Analysis of the texture is done with the help of the Orientation Distribution Function (ODF) that is calculated by the MTM FHM program of van Houtte (van Houtte, 1992) based on the pole figures (110), (200) and (211). The ODF shows the distribution of the 3 subsequent rotations that are necessary to rotate the coordinate system of the sample to the coordinate system of each crystal, detailed information can be found in Bunge (1993).

3.3. Rolling trials

Both the rolling experiments and the sample preparation were done on the pilot mill of Tata Steel in IJmuiden, see Fig. 4 for a schematic overview and photo of the mill.

The lower the plane strain factor, the less negative the vertical pressure in the roll bite (according to Eq. 8) and the lower the rolling force. To show that the plane strain factor is overestimated by the von Mises yield criterion, it suffices to show that the rolling force according to the model is higher than in the experiment. This is not straightforward, as also the friction influences the rolling force and the friction is

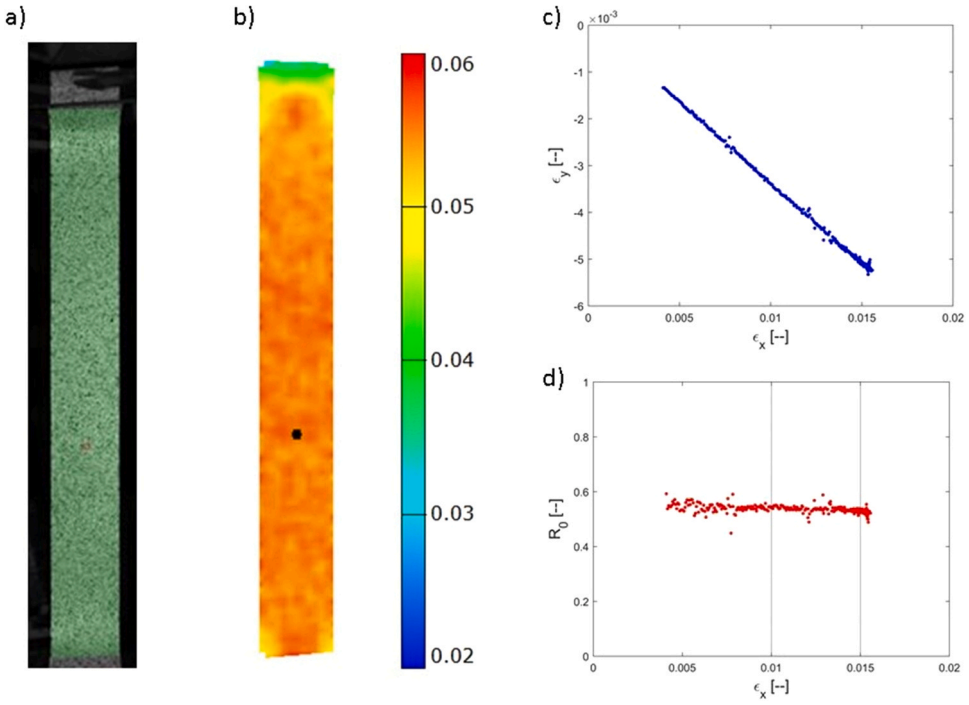

Fig. 3. Visualisation of ARAMIS results. a) in-situ photo of speckled tensile sample, b) distribution of longitudinal strain over test sample, c) measured transversal strain versus measured longitudinal strain, d) calculated R_0-value as function of longitudinal strain, the presented R_0-value is the average between the two vertical lines. In a) en b) the dot indicates the reference point around which the area of interest is defined.

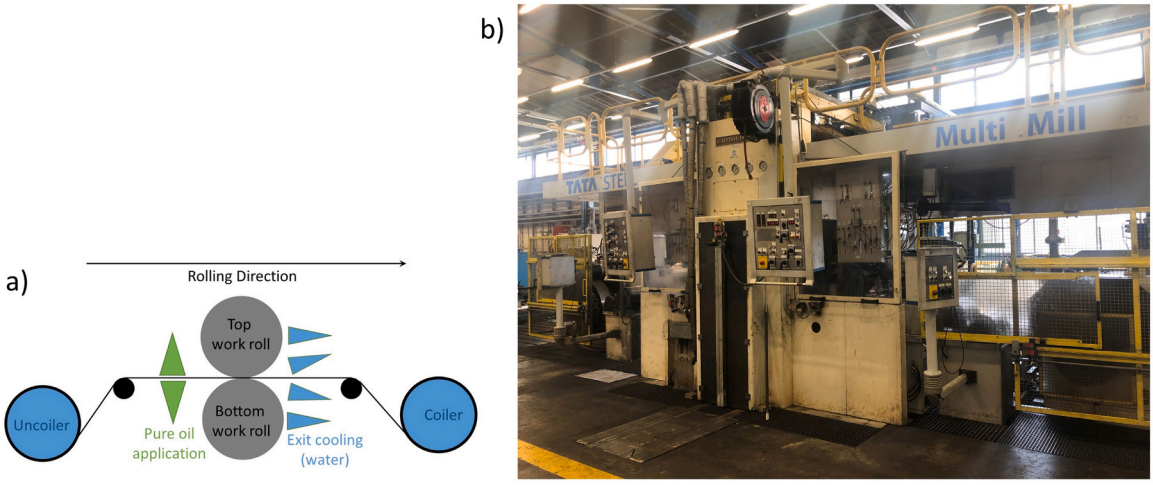

Fig. 4. a) Schematic configuration of pilot mill as used during the rolling trials, b) photo of pilot mill.

not known quantitatively. Therefore, the aim of the rolling experiments is to show that the measured rolling force is even lower than the lowest possible model outcome, which is achieved by extrapolating the predicted rolling force for $\mu \rightarrow 0$. In order to experimentally approach this minimum solution as good as possible, the trials were carried out with relatively smooth work rolls (diameter = 400 mm, R_a-value = 0.1 μm) and were lubricated with neat oil, so that lubrication will be primarily in the hydrodynamic lubrication regime and the coefficient of friction is low. Furthermore, a combination of entry/exit tension is chosen such that the exit tension draws the material in the roll bite, enabling the model to find a solution even for low values of the coefficient of friction. The strip roughness was also low, the R_a-value ranged between 0.3 and 0.6 μm in the center of the coil.

Eleven different rolling passes were carried out, all relevant rolling parameters are shown in Table 1. The rolled coils were long enough to make flying changes in speed or tension within one rolling pass. This allowed to carry out multiple processes within a single rolling pass and increase the statistical significance of the results. Pass 4 of grade A is rolled at constant rolling force (650 kN), other passes are run in mass-flow control towards the aimed strip thickness.

As shown in Section 4.3, the measured rolling force for coil A was extremely low. To be absolutely sure of the measurement accuracy, between coil A and B the rolling force measurement of the pilot mill was calibrated against a certified pressure gauge. The calibration showed that the rolling force was accurately measured during the entire trial.

Table 1
Rolling schedule. First passes serving to smoothen the strip, are not shown. In between pass A1-A2, A2-A3, B3-B4 and pass B4-B5 a small pass was inserted to smoothen and level the strip again. These intermediate passes are not relevant for the trial and are not shown in this table.

Steel grade Pass nr	Oil type	t_{in} (mm)	t_{out} (mm)	v_{roll} (m/s)	σ_{entry} (MPa)	σ_{exit} (MPa)
A-1	1	1.40	1.20	2	205–97 (3 steps)	164–320 (3 steps)
A-2	1	1.10	1.00	2	234–114 (3 steps)	201–353 (3 steps)
A-3	1	0.90	0.80	0.1–2 (6 steps)	141	292
A-4	1	0.80	0.61	7	54–123 (7 steps)	165
B-1	2	1.20	1.10	1–7 (7 steps)	27	90
B-2	2	1.10	1.00	1–7 (7 steps)	30	100
B-3	2	1.00	0.90	1–8 (7 steps)	33	111
B-4	2	0.85	0.75	1–7 (7 steps)	37	133
B-5	2	0.70	0.55	2–8 (4 steps)	45	181
B-6	2	0.55	0.45	3–9 (4 steps)	56	221
B-7	2	0.45	0.35	3–10 (5 steps)	70	285

3.4. Samples

Two different low-carbon grades were studied in this work, grade A and grade B. The initial strip width was 100 mm and the initial strip thickness was 2.4 mm and 2.0 mm for grade A and B respectively. The chemical composition (target or maximum value) of both steel grades is shown in Table 2.

The original objective of the rolling trial with coil A was not to investigate anisotropic yielding behaviour. Therefore relatively few tensile tests were carried out to determine the R_0-value on grade A, furthermore the ARAMIS was not used yet during tensile testing of grade A and also the XRD-measurement were only performed on grade B.

Samples for XRD and tensile tests for grade B were obtained by cold rolling coils on the pilot mill to final gauges of 1.98 mm, 1.90 mm, 1.80 mm, 1.60 mm, 1.20 mm, 0.65 mm and 0.40 mm which represent thickness reductions of 1 %, 5 %, 10 %, 20 %, 40 %, 67 % and 80 % respectively. For the tensile tests, both ASTM25 and A80 tensile samples were prepared. As shown in Section 2.1, only the R_0 is relevant for the cold rolling process, therefore the length direction of all tensile samples corresponds with the rolling direction. For the crystallographic texture measurements, samples were prepared of 30 × 20 mm.

4. Results

In this section it is shown experimentally that the steel grades considered in this study become strongly anisotropic due to the cold rolling process and that this anisotropy has a significant influence on the rolling force during cold rolling.

Table 2
Chemical composition (in weight percent) of the investigated steel grades.

	C	Mn	Al (soluble)	P	S
Grade A	0.070	0.400	0.015	<0.020	<0.012
Grade B	0.075	0.350	0.040	<0.020	<0.020

4.1. Tensile tests

Both for grade A and B, the results of the tensile tests are shown in Fig. 5. Fig. 5a presents the work hardening behaviour of both steel grades, tensile test results are the average of 2–4 individual measurements with a typical standard deviation of 8 MPa. The tensile test results are in good agreement with the model described by van Liempt (1994) which is shown as well. The corresponding Bergstrom-van Liempt model parameters are given in Table 3. These stress-strain curves, complemented with the appropriate viscoplastic behaviour described by Krabiell and Dahl (1981), is used to analyse the rolling experiments described in Section 4.3.

Fig. 5b clearly shows that the R_0-value for grade B decreases during cold rolling from almost isotropic before cold rolling to $R_0 \approx 0.5$ after 80 % reduction. For grade A there are only results for higher cold rolling reductions, again with R_0-values significantly lower than 1. This is indicative of an important normal anisotropy, resulting in a lower *PS* -factor according to Fig. 1b. For grade B, the R_0-value is determined directly by the Zwick/Roell tensile tester as well as with the ARAMIS, both results are shown in Fig. 5b. Typical standard deviations are lower with the ARAMIS (0.04 compared to 0.08 for the R_0-value determined by the Zwick/Roell tester); therefore, the R_0-values as determined by the ARAMIS will be used in this work for further analysis of the anisotropic material behaviour.

4.2. Crystallographic texture

The crystallographic texture is analysed by means of the Orientation Distribution Function (ODF), which shows the frequency of the crystal orientations in the sample. Because for ferritic steels all major texture components are represented in the $\varphi_2 = 45^\circ$ cross section of the ODF (for example Tamimi et al., 2018), this cross section is shown in Fig. 6 for all samples.

Fig. 6 shows that even from low cold rolling reductions there is a clear development of texture towards intense α-fibre and γ-fibre at 80 % of cold rolling reduction.

Based on the measured textures, the model developed by van Houtte (1992) is used to estimate the R_α-value, these results are shown in Fig. 7a. The van Houtte model also determines directly the Plane Strain factor as a function of the direction, these results are shown in Fig. 7b.

As cold rolling is almost a perfect plane strain process, only the $\alpha = 0$ direction is relevant in this work. According to Fig. 7a also the initial (hot rolled) material is not completely isotropic but $R_0 \approx 0.9$; with increasing cold rolling reduction the R_0-value decreases to approximately 0.5 for a sample with 80 % reduction. A surprising result is that the relation between calculated R_0-value and *PS*-factor deviates from Eq. 9 (and therefore also from the experimental results of Abspoel et al. (2017) in Fig. 2a), this is shown explicitly in Fig. 8a. Fig. 7b demonstrates that the calculated plane strain factor decreases with increasing cold rolling reduction; however, the plane strain factor varies less than could be expected based on Eq. 9. This will be further addressed in the discussion section.

Table 3
Bergstrom-van Liempt parameters for the material used in the experiments.

Parameter	Grade A	Grade B	Units
σ_0	148	274	MPa
α_{BL}	0.82	0.82	–
G	$78{\cdot}10^3$	$79{\cdot}10^3$	MPa
b	$2.5{\cdot}10^{-10}$	$2.5{\cdot}10^{-10}$	M
U	$2.81{\cdot}10^8$	$1.44{\cdot}10^8$	m/m^2
Ω	9.79	4.25	–
β	0.174	0.155	–
ρ_0	$2{\cdot}10^{13}$	$1{\cdot}10^{12}$	m/m^3
$\sigma_{dyn,0}$	1228	1229	MPa
k	$8.617{\cdot}10^{-5}$	$8.617{\cdot}10^{-5}$	eV/K
ΔG_0	0.97	0.97	eV
$\dot{\varepsilon}_0$	$4.63{\cdot}10^{10}$	$4.63{\cdot}10^{10}$	s^{-1}
r	3.38	3.38	–

The complete development of the calculated yield loci as a function of cold rolling reduction is shown in Fig. 8b. This graph is made by normalizing all results on the yield stress for uniaxial tension in the rolling direction. The graph therefore clearly shows the change of the contour of the yield locus with varying cold rolling reduction. According to experts in the field (i.e. Van Houtte et al., 1989) the shape of the yield locus is strain rate (and temperature) independent.

Fig. 9 compares the R_0-value and *PS*-factor obtained for grade B from the van Houtte model (based on the measured crystallographic texture) with the R_0-values from the tensile tests (ARAMIS results) and the resulting *PS* -factor by using the Hill48 criterion. As a reference, in both graphs also the values according to the isotropic von Mises yield criterion are given.

Fig. 9 clearly shows that the material behaviour is not well described by the isotropic von Mises yield criterion: both independent experiments indicate a significant anisotropic yielding behaviour. The ARAMIS results in Fig. 9 are the average value of 3 tensile tests (one ASTM25 and two A80 samples), the standard deviation is typically 0.04 which indicates that the differences with isotropic behaviour are statistically significant.

Fig. 9 shows a notable difference between the two experimental methods. In Section 5, a cold rolling model is used to determine the influence of anisotropic material yielding on rolling force which makes it plausible that the tensile test results are more accurate. As only rolling

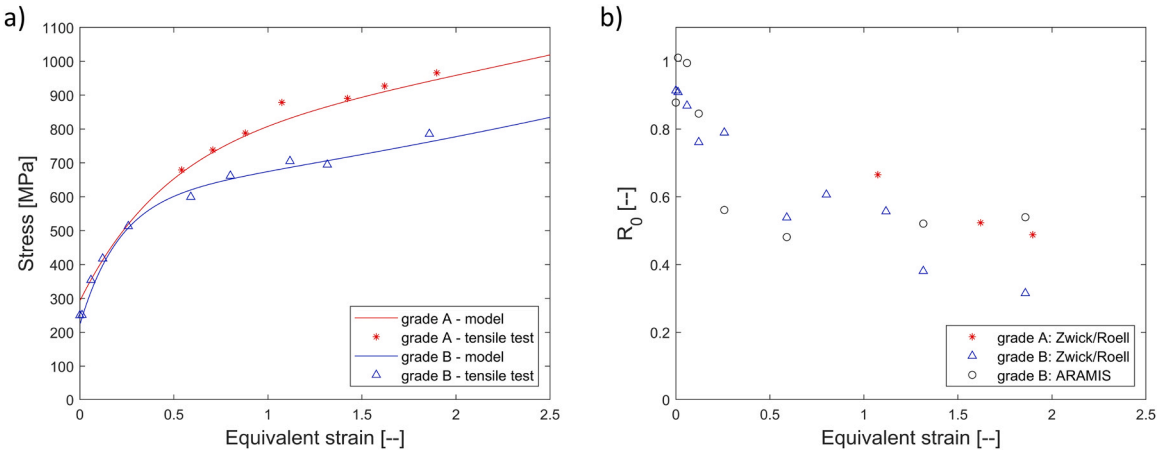

Fig. 5. Results of tensile tests. a) Rp-value of grade A and B as function of equivalent strain, both model results and tensile test results. b) R_0-value of grade A and B as function of equivalent strain, as determined from tensile tests, both by ARAMIS system as well as the Zwick/Roell tensile tester.

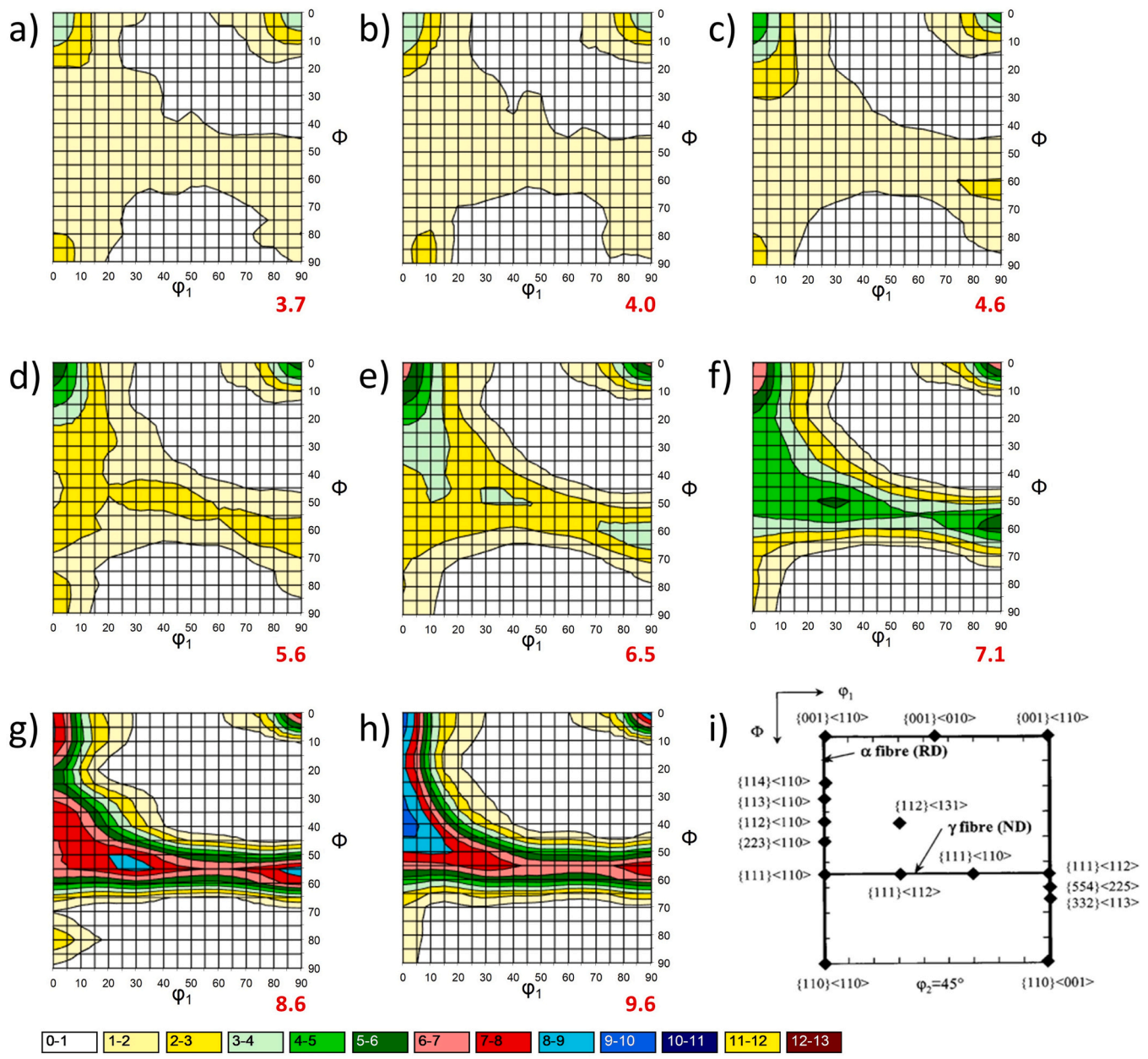

Fig. 6. a-h) φ_2=45° Cross section of the measured ODF, for the samples withrespectively 0, 1, 5, 10, 20, 40, 67 and 80 % of cold rolling reduction, i) main components and fibres in the φ_2=45° cross section of the ODF for a BCC crystal like ferrite (adaptedfrom Waterschoot et al., 2002). At the bottom the colorlegend for the contour lines is given, the maximum intensity is given in red atthe bottom of each ODF.

processes are considered with $\varepsilon_{equiv} > 0.5$, the fits indicated in Fig. 9 are an accurate representation of the measurements and will be used as input to this rolling model. For grade A there are not enough experimental results to deduce a reliable fit. The few available results suggest that the R_0-value is very similar for grade A and B, therefore the same fit is used to quantify the anisotropic yielding behaviour for both grades.

Fig. 9b shows that according to the tensile tests (combined with the Hill48 criterion), the *PS*-factor for the material with 80 % reduction is approximately 9 % lower than the *PS*-factor according to the von Mises criterion. This has a significant influence on the calculation of rolling force by the rolling model, which will be further demonstrated in Section 5.1.

4.3. Rolling trials

In the previous two sections it was shown that during cold rolling the crystallographic texture changes significantly. Calculations (based on this texture) as well as tensile test results indicate that this results in anisotropic material behaviour characterized by R_0 lower than 1. In this section it will be shown that this effect plays a significant part in cold rolling of steel.

The measured rolling force of the first pass of both coils is shown in Fig. 10, it is compared with rolling model calculations (described in Section 2.2) for different coefficients of friction.

Especially for grade B (Fig. 10b), the measured rolling force is lower than the predicted rolling force, even if the results are extrapolated to $\mu = 0$ (the model does not converge for unrealistically low coefficient of friction such as $\mu = 0$). This means in the model, the correct rolling force can only be achieved by using a negative COF, which clearly has no physical meaning. Other critical parts of the rolling model are experimentally validated (like the elastic work roll flattening by Jacobs et al., 2022), or validated against more advanced models (like using the

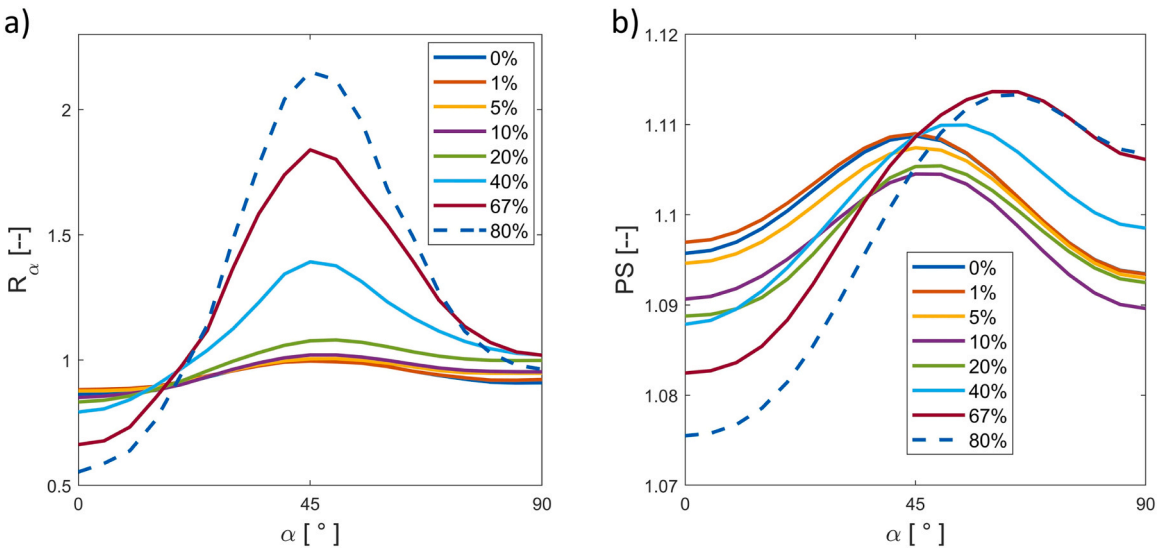

Fig. 7. a) Calculated R_α-value as function of the angle with the rolling direction for different cold rolling reductions, b) calculated *PS*- factor as function of the angle with the rolling direction and cold rolling reduction.

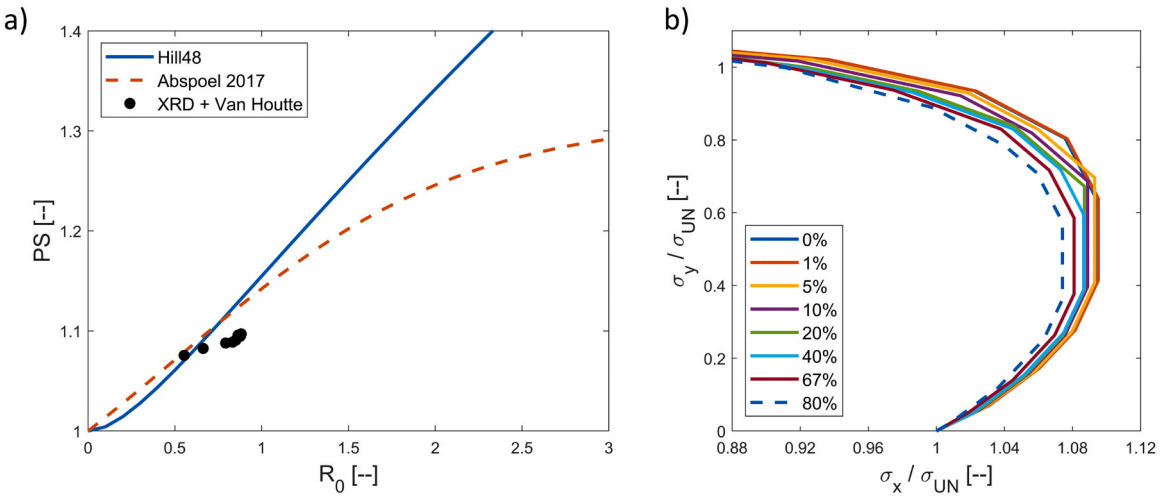

Fig. 8. a) Comparison of van Houtte model (based on XRD-results) with the results of Abspoel et al. (2017) and the Hill48 criterion. b) development of yield loci (as calculated from XRD-results) as function of cold rolling reduction.

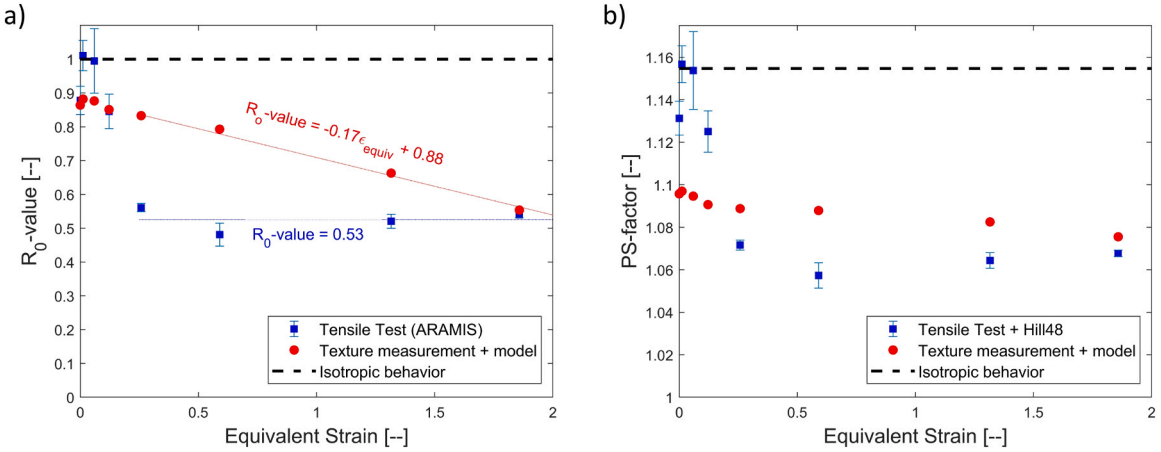

Fig. 9. Comparison of experimental results: anisotropic material behaviour of grade B according to tensile test (+Hill48 model) and XRD-measurements (+ van Houtte model). a) R_0-value as function of the cold rolling reduction, b) *PS*-factor as function of the cold rolling reduction. Vertical error bars correspond to one standard deviation.

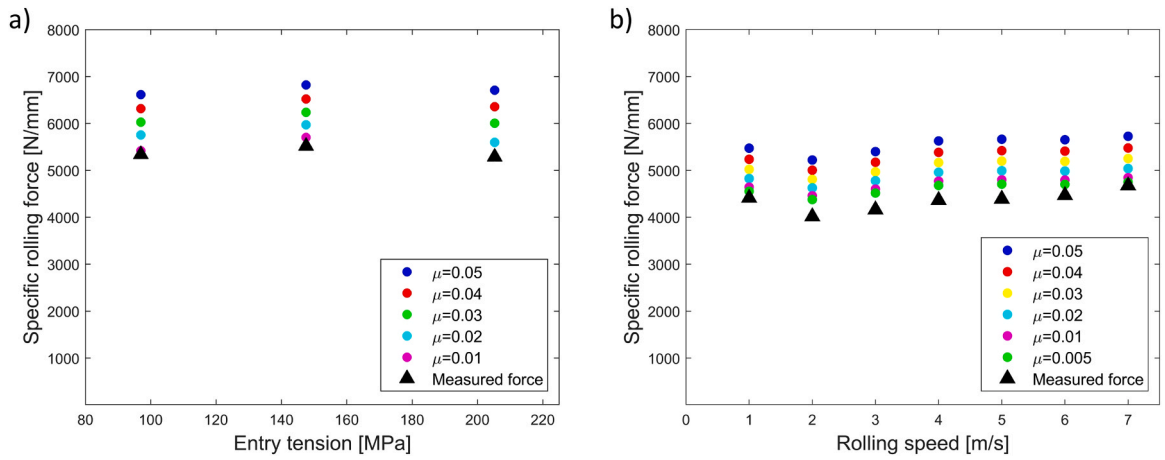

Fig. 10. a) Results pass 1 with grade A: rolling force versus entry tension, comparison of measured values with model predictions (with different COF). b) results pass 1 with grade B: rolling force versus rolling speed, comparison of measured values with model predictions.

slab-method in cold rolling by Montmitonnet, 2006). Usually friction is the unknown parameter in a cold rolling experiment or simulation, but here only the lower bound for $\mu = 0$ is used, therefore clearly something else is missing in the model. These results thus strongly suggest that the strip yield point is overestimated in the rolling model.

The experimental results for grade A (Fig. 10a) can be reproduced by the rolling model but only with unrealistically low COF ($\mu \approx 0.003$). Although the experiment was designed to achieve a low COF (in order to be close to the lower bound of the rolling model), such low COF is unlikely to be achieved in a rolling experiment even if carried out under hydrodynamic rolling conditions. Therefore these results also strongly suggest that the material yield point is overestimated in the model.

The results of pass 1 (Fig. 10) are representative for the entire trial: both with grade A and with grade B, for some passes the measured rolling force is lower than the model can possibly predict and for some passes the measured results can only be matched when an unrealistically low coefficient of friction is used in the rolling model. According to Yuen et al. (1996b) the COF in rolling is typically between 0.015 and 0.06. In each and every pass of this experiment, the necessary COF to match the measured rolling force is smaller than 0.015.

It follows directly from the von Karman equation that the influence of friction on rolling force is higher for thin material (for example Azushima, 2015). The larger influence of friction on rolling force in pass 7 of grade B is visualized in Fig. 11 by the higher increase of calculated rolling force for a given increase in COF. This means that for thin material the relative influence of mechanical properties on rolling force decreases. Consequently, for this case the measured rolling force can be matched by using a realistic, albeit still very low, COF in the model namely $\mu \approx 0.01$. The results in Fig. 11 are representative for the last three passes with grade B. Appendix A shows a comparison of measured rolling force with model results for every pass of the rolling trial.

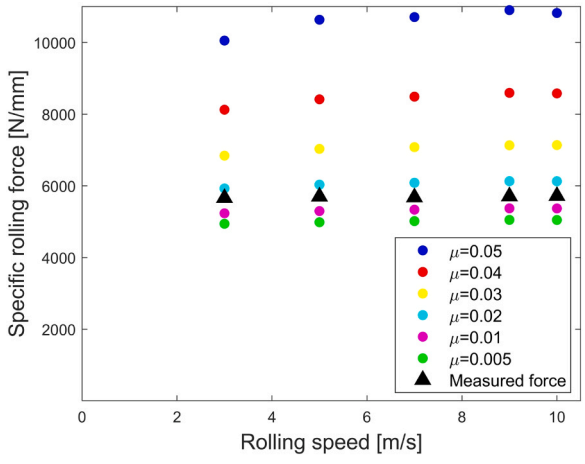

Fig. 11. Results pass 7 with grade B: rolling force versus rolling speed, comparison of measured values with model predictions (with different COF).

5. Discussion

5.1. Impact of anisotropic yielding in cold rolling

It is not within the scope of this work to present a complete cold rolling model. Instead, the objective of this work is to show that anisotropic material behaviour has a significant influence on the cold rolling force. This has been shown in the rolling experiments where the influence of friction was made as small as possible.

In this section, the same rolling model is used to illustrate the effect of anisotropic material behaviour in more realistic industrial rolling conditions, for rolling processes with an industrially common work roll roughness (and corresponding coefficient of friction). Fig. 12a shows the calculated influence of yield anisotropy by comparing model results with R_0-values of 1.0 and 0.5. For the chosen rolling process, the difference in calculated rolling force is 15 %. This difference is due to the 9 % difference in *PS* -factor and other 2nd order effects such as the higher shear stresses and increased work roll flattening, both due to higher vertical pressure when $R_0 = 1$ compared to $R_0 = 0.5$.

The difference in predicted rolling force between anisotropic and isotropic material is very high, which justifies the question how it has been possible up to now to use cold rolling models based on isotropic material behaviour to accurately predict the cold rolling process. Therefore the same calculation is repeated but for isotropic material behaviour with a lower COF ($\mu = 0.038$). Fig. 12b shows that it is possible to achieve a friction hill that is rather similar to the anisotropic model calculation. The rolling force for both calculations in Fig. 12b is equal, only the neutral point position is slightly different. Apparently, cold rolling models based on the isotropic von Mises criterion can predict rather accurately the friction hill but the coefficient of friction that must be used is lower than in reality. This demonstrates that the commonly applied method of back-calculating the coefficient of friction (by fitting with the rolling force), has hidden the influence of material anisotropy. Based on this discussion, it can be concluded that:

- A rolling model with the von Mises yield criterion only takes isotropic material behaviour into account. If such a model is used and

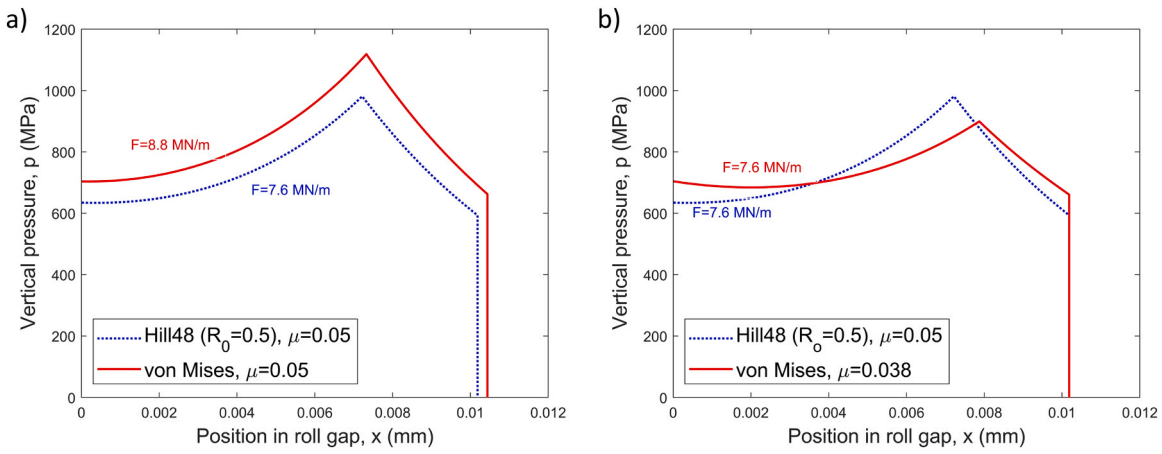

Fig. 12. Friction hill calculation of rolling models with different degree of anisotropic yielding and coefficient of friction. a) difference between anisotropic yielding (R_0=0.5 vs. R_0=1) with the same COF. b) difference between anisotropic yielding (R_0=0.5 and R_0=1), COF chosen so that the rolling force is equal. Rolling parameters were arbitrarily chosen ($t_{in} = 1mm, t_{out} = 0.65mm, v_{roll} = 2m/s, r_0 = 0.2m, \sigma_{in} = \sigma_{out} = 150MPa, \mu = 0.05$ while the work hardening properties of grade B were used).

the material behaviour in reality is anisotropic, the back-calculated coefficient of friction is lower than in reality.

- Empirical knowledge of the coefficient of friction during rolling is mostly based on back-calculation from experiments with models based on isotropic material behaviour. For example, Yuen et al. (1996b) derive that the coefficient of friction during rolling of low-carbon steel ranges normally between 0.015 and 0.06. However, if anisotropic material yielding is taken into account, the back-calculated friction forces would be higher. A more realistic estimation of the coefficient of friction is between 0.03 and 0.08.
- Mixed lubrication models, such as detailed in Boemer (2020), describe friction on a more physical basis. Using such physically based lubrication models only makes sense if also the correct (anisotropic) material behaviour is taken into account.

It follows that for an accurate prediction of the friction hill, the anisotropic yielding behaviour of the steel must be taken into account. Most likely this behaviour differs per steel grade: Moerman (2005) measured the development of crystallographic texture for an Interstitial-Free steel grade. His results show that such steel grades have a very strong texture, even in the hot-rolled stage. A predictive model for the degree of normal anisotropy seems therefore necessary. As mentioned in the introduction, many researchers have worked on models to predict the development of the crystallographic texture during cold rolling, with the objective to optimise final product properties. The degree of physics in these models varies: Brahme et al. (2009) and Das (2017) use neural networks, while Takajo et al. (2019) use a viscoplastic self-consistent poly-crystal model where each grain is considered as an ellipsoidally shaped inclusion while the rest of the matrix is considered as a homogeneous medium. Deeperekha et al. (2020) use full field crystal plasticity models that are computationally very efficient to determine the evolution of texture.

Industrial cold rolling setup models usually rely heavily on coil-to-coil adaptation on the coefficient of friction (for example Pires et al., 2009). If anisotropic yielding behaviour is not taken into account accurately by the model, this will negatively influence the accuracy of the back-calculation of the coefficient of friction and impair the coil-to-coil adaption. Even if more advanced, self-learning, methods are used for adaptation, it is beneficial to include anisotropic plastic yielding in the cold rolling model to increase its accuracy as much as possible.

Besides rolling force, also the forward slip is an important output parameter of a cold rolling model. Taking anisotropic yielding into account in the cold rolling model has little influence on the forward slip. In the simulation results shown in Fig. 12a, the neutral point position is almost equal for R_0= 0.5 and R_0= 1. More generally, material properties only have limited influence on the forward slip (according to Liu et al., 2001, forward slip depends primarily only on strip thickness, work roll radius and coefficient of friction). It can be deduced that to improve the forward slip prediction, especially the description of friction in the roll bite must be improved.

A final remark related to the impact of anisotropic plastic yielding is that most likely its occurrence is not restricted to cold strip rolling of low-carbon steel. Because of the nature of the process, it is very likely that anisotropic material behaviour is also present during cold strip rolling of other metals. Presumably, it is even more important in the cold rolling of bars, because then it not only influences the rolling force but also the lateral material flow.

5.2. Suitability of Hill48 yield criterion for cold rolling

This work proposes to use the Hill48 yield criterion to translate the uniaxial tensile test result to plane strain conditions that are prevalent during cold rolling. Besides the obvious different location on the yield locus, another difference is that the uniaxial tensile test is carried out under hydrostatic tension ($\sigma_{hydr} = \sigma_{UN,yield}/3$) while cold rolling is carried out under hydrostatic pressure ($\sigma_{hydr} \approx -\sigma_{UN,yield}/2$). In this section the suitability of the Hill48 criterion to account for these differences is discussed.

Fig. 5 shows that cold rolled material is characterized by a low Lankford parameter, this means that the plane strain yield point is very close to the uniaxial yield point (see Fig. 1a). This makes it likely that the plane strain yield point can be accurately estimated from the uniaxial yield point as is illustrated here. For high values of the Lankford parameter, the plane strain and uniaxial yield point are further apart and more complex yield functions are necessary for an accurate prediction of the plane strain yield point. This is confirmed by the experimental results of Abspoel et al. (2017) in Fig. 2, which show that only for Lankford parameters smaller than 1 there is good agreement between the *PS* -factor predicted by Hill48 and experiments. It can be concluded that the Hill48 criterion is suitable to account for the different location of the yield point between the tensile test and cold rolling.

The yield loci shown in Figs. 1a and 8 reflect yielding under plane stress conditions ($\sigma_y = 0$). Both the von Mises criterion and the Hill48 criterion depend only on stress deviators and not on hydrostatic pressure. This is used to translate the yield loci under plane stress to yielding conditions during cold rolling. For high-strength martensitic steel grades however, Spitzig and Richmond (1984) find that the yield stress increases with hydrostatic pressure. Because of this, the yield stress during

cold rolling is a few percent higher than for $\sigma_y = 0$. This results in the so called Stress Differential Effect (SDE) that increases the vertical pressure in the roll bite. This effect should therefore be considered in cold rolling models for martensitic steel grades. For low-carbon grades however, Watt and Jain (1984) indicate that "*strength differentials are not observed in annealed ferrite, nor in equiaxed ferrite-pearlite microstructures*" and according to Koizumi and Kuroda (2018) also an interstitial free steel grade does exhibit almost no SDE. This seems to correspond to the current consensus that normal, single phase, low-carbon steels exhibit almost no SDE. Also in the standard book of Lange (2002), varying the hydrostatic pressure does only marginally change the yielding condition.

It can be concluded that for single phase low-carbon steel grades, the Hill48 criterion is suitable to account for the differences in the uniaxial tensile test and the cold rolling process.

5.3. Quantification of anisotropic yielding from cold rolling trials

A first point of discussion is the significant difference of R_0-values presented in this work for cold rolled material and the R_0-values for cold rolled and annealed material (for example Hutchinson and Artymowicz, 2001 present average R-values higher than 2). Hutchinson and Ryde (1997) clearly show the differences in crystallographic texture between cold rolled material and cold rolled plus annealed material. For cold rolled material they find a strong alpha fibre (i.e. {hkl}⟨110⟩) including a strong rotated cube (i.e. {001}⟨110⟩) and a slightly less strong gamma fibre (i.e. {111}⟨uvw⟩), which all corresponds to the XRD-results shown in Fig. 6h. After recrystallization they find mainly a strong gamma fibre. The formation mechanisms of recrystallized texture from cold rolling texture is discussed in detail by Inagaki (1994). The completely different anistropic material behaviour after annealing comes from this difference in crystallographic texture.

A further point of discussion is that the Taylor-based van Houtte model underestimates the influence of texture on R_0-value and PS -factor (compared with the tensile tests and the Hill48 criterion). Fig. 9 shows that according to the tensile tests the R_0-value and hence the PS -factor are lower than according to the model results. The cold rolling model, now including anisotropic yielding behaviour according to the results presented in Fig. 9, can be used to assess which description of anisotropic yielding behaviour is more realistic. Fig. 13 shows the measured rolling force compared with model results including material anisotropy according to Van Houtte et al. (1989); the measured rolling force in the first rolling pass is still lower than the model results with $\mu = 0$. Apparently the anisotropic yielding in the first pass is still underestimated.

On the contrary, using the R_0-value as obtained from the tensile tests in the cold rolling model results in a good agreement between experimental observations and model results for a plausible coefficient of friction. In Fig. 14 the measured rolling force is compared with the model results for the first and last rolling pass with grade B.

Fig. 14 shows that the measured rolling force in the first pass corresponds with the model results for μ≈0.015–0.030, what is a plausible level. The rolling force in the last pass also corresponds to model results for μ≈0.025. These results are representative for all other rolling passes: all measured rolling forces correspond with model results for μ ranging from 0.015 to 0.03.

Because all passes are lubricated under the same conditions (the variation in lubricant temperature or strip roughness were relatively small between the passes, while the thickness reduction was mostly 0.1 mm), a somewhat similar COF is indeed expected for all passes. This is only the case when the R_0-value as obtained from the tensile tests is used in the cold rolling model. Furthermore, a value of μ≈0.025 is a very realistic value for a well-lubricated process that is (almost) in the hydrodynamic lubrication regime.

A possible explanation for the observed difference in R_0-value between tensile tests and van Houtte model is that the mid-thickness crystallographic texture is not representative for the entire sample: a texture gradient over the thickness may be present, for example due to applied shear at the surface during cold rolling. This explanation corresponds to the result that the R_0-value following from the tensile tests performs better in the rolling model, as this value should be an average over the entire strip thickness. To further investigate this, it could be interesting to measure the gradient of crystallographic texture over the strip thickness as was done for example by Zhou et al. (2018) on Aluminium.

Due to elastic recovery of the strip, the strip-roll contact length is usually longer than it would be for perfect plastic material. However, both theoretical as well as experimental studies have shown this effect to be relatively small. Jacobs et al. (2022) observed the contact length with a camera and concluded it corresponds well with the theory based on perfect plastic material and Hitchcock work roll flattening. Li et al. (2018) drew similar conclusions, especially for thickness reduction smaller than 20 %, based on the shape analysis of half-rolled strip samples. Baranov and Ilin (2022) concluded that, for strip rolling process with more than 10 % thickness reduction (as is the case in the experiments presented in this work), the extra contact length due to elastic recovery is less than 5 %. At the end of the elastic recovery zone the vertical pressure must have dropped to zero. The influence of elastic strip recovery on rolling force is therefore less than its influence on contact length, based on the results in abovementioned references it should be less than 3 %. Fig. 12 shows that an overestimation of the

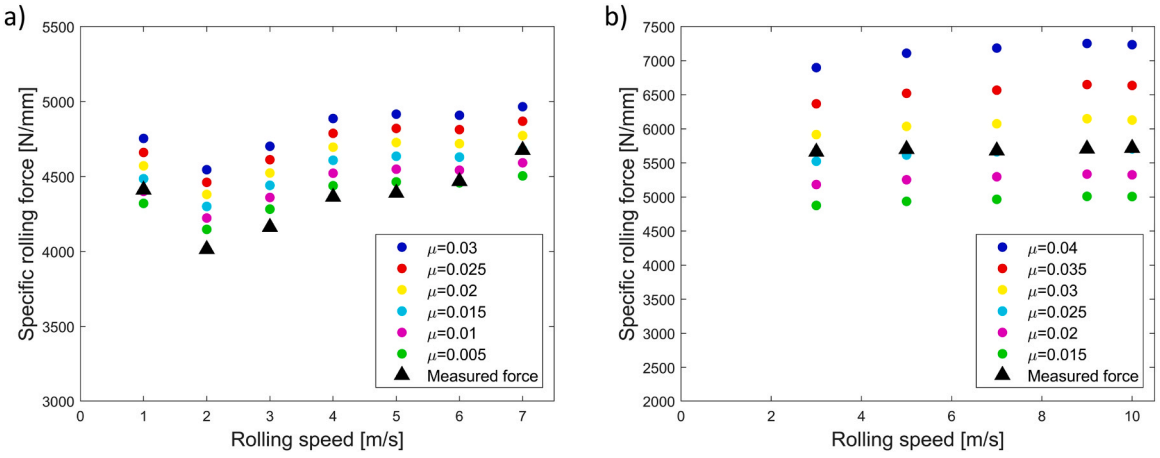

Fig. 13. Rolling force versus rolling speed, comparison of measured values with model predictions (different COF). Model now includes R_0-value according to XRD-experiments combined with van Houtte model. a) pass 1 grade B, b) pass 7 grade B.

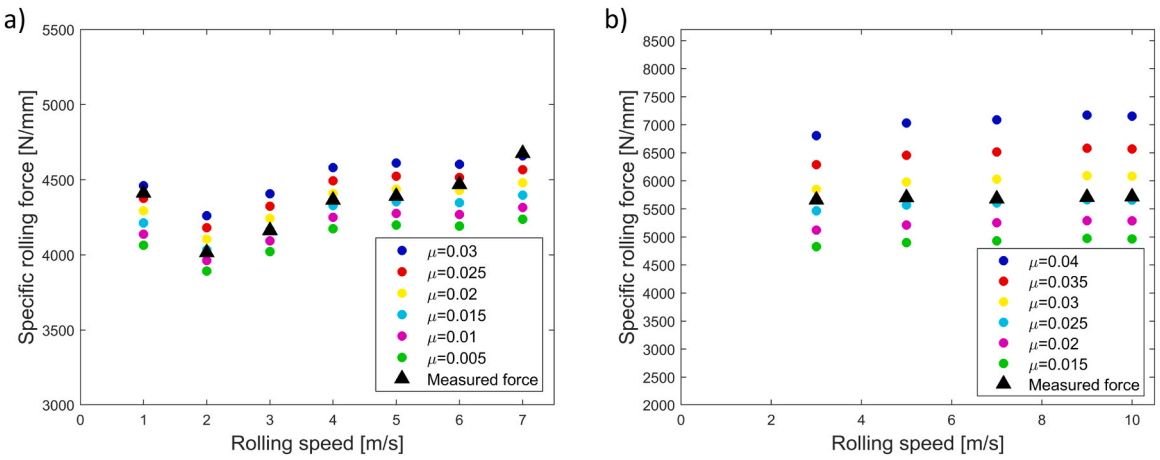

Fig. 14. Rolling force versus rolling speed, comparison of measured values with model predictions (different COF). Model now includes R_0-value according to ARAMIS analyis of tensile tests. a) pass 1 grade B, b) pass 7 grade B.

rolling force by 15 % can be offset by a decrease in coefficient of friction of approximately 0.01; it can be derived that a model that does not take elastic strip recovery into account, overestimates the coefficient of friction by 0.001–0.002. It can be concluded that neglecting elastic strip recovery has not significantly influenced the results presented in Figs. 10, 11, 13 and 14 as well as the figures in the appendix.

As a last step, the accuracy of the rolling force prediction is determined by comparing the measured rolling force with model prediction for all experiments described in Table 1 (including all process variations that were done within one pass). As these processes were carried out with the same smooth work rolls and with pure oil application, it is expected that all processes are (almost) in the hydrodynamic lubrication regime. Therefore the actual coefficient of friction is expected to be low and rather similar for all processes. This optimum COF is determined by back-calculation: it is the value that (on average) gives the best rolling force prediction.

The optimum COF is then used to determine the rolling force for all rolling processes in Table 1. To enable a good comparison, only processes are considered that converge both when anisotropic as well as isotropic material behaviour are used in the rolling model. The predicted rolling force is plotted against the measured rolling force in Fig. 15. An overview of the optimum coefficient of friction and the average error in rolling force prediction is given in Table 4. Fig. 15 shows that with this optimum COF, the model that accounts for anisotropic yielding predicts the rolling force for all processes quite accurately. The prediction accuracy with the model based on isotropic yielding is much lower.

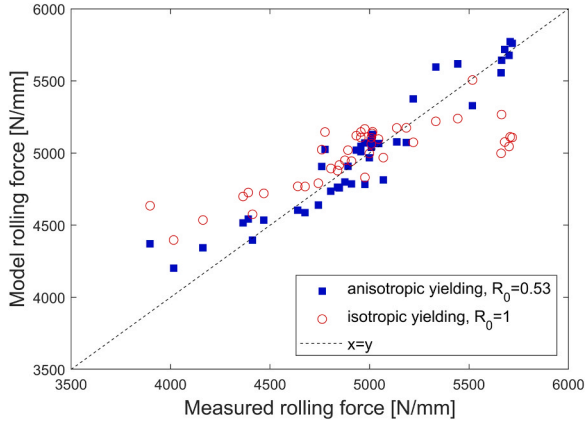

Fig. 15. Comparison of simulated rolling force with measured rolling force for the processes defined in Table 1, both for the rolling model based on isotropic and anisotropic material yielding.

Table 4
Summary of model results with anisotropic/isotropic material yielding.

	Optimum COF	Average error
Model with anisotropic yielding (R_0=0.53)	0.026	2.5 %
Model with isotropic yielding (R_0=1)	0.006	4.7 %

The results of these model simulations therefore confirm the benefits of taking anisotropic yielding into account in the cold rolling model:

- The optimum COF for all processes described in Table 1 is 0.026, which is a plausible value for a cold rolling process that is (almost) in the hydrodynamic lubrication regime. On the contrary, the optimum COF when anisotropic yielding is not considered is only 0.006. This value is unrealistically low, even for a well lubricated cold rolling process.
- For the rolling processes described in Table 1, the average error in rolling force prediction improves from 4.7 % to 2.5 % by taking anisotropic material yielding into account in the cold rolling model.
- While the model based on isotropic yielding does not converge for some rolling processes, the model with anisotropic yielding converges for 100 % of the processes described in Table 1.

6. Conclusions

This article quantifies anisotropic material yielding behaviour during cold rolling and its influence on rolling force. The following conclusions can be drawn from this work:

- It is important to take anisotropic material behaviour into account in cold rolling models. Normal anisotropy influences the plane strain condition during rolling and consequently it influences the vertical pressure and the rolling force.
- Both crystallographic texture measurements and tensile test results indicate that cold rolled low-carbon steel exhibits anisotropic yielding behaviour. For the grades investigated in this work, the R_0-value decreases from almost 1 for the initial material to approximately 0.5 for the sample with 80 % cold rolling reduction. Consequently the plane strain factor of the sample with 80 % cold rolling reduction is approximately 9 % lower than predicted by the isotropic von Mises yield criterion.
- The most widely used cold rolling models, so called slab models, assume isotropic material yielding. These models can describe the rolling process accurately, but only if an underestimated coefficient of friction is used. The inaccuracy in description of material plasticity

is thus compensated by another inaccuracy in the friction behaviour. It is shown that the real coefficient of friction in the cold rolling process is approximately 0.01 higher than back-calculated values. This conclusion can lead to new insights related to tribology in cold rolling.

- The effect of anisotropy is confirmed in cold rolling experiments. The observed rolling force in these experiments was so low that the measured rolling force can only be predicted using an unrealistically low, or even negative, coefficient of friction in a cold rolling model that assumes isotropic material behaviour.
- If the cold rolling slab model is extended with the Hill48 criterion, it can account for anisotropic material yielding. With this new rolling model, the measured rolling force corresponds much better with model results.

CRediT authorship contribution statement

L.J.M. Jacobs: Conceptualization, Methodology, Investigation, Validation, Writing – original draft. **E.H. Atzema:** Methodology, Writing – review & editing. **J. Moerman:** Methodology, Investigation, Writing – review & editing. **M.B. de Rooij:** Conceptualisation, Supervision, Project administration, Writing – review & editing.

Declaration of Competing Interest

The authors declare that they have no known competing financial interests or personal relationships that could have appeared to influence the work reported in this paper.

Data Availability

Data will be made available on request.

Acknowledgements

The work presented in this article involved much experimental work. The authors gratefully thank Frank van der Does for preparation of the XRD-samples, Stefan Melzer for the texture measurements, Frank Schouten, Ferry Zwaan and Nick Ontijt for setting up and carrying out the tensile tests and Daphne van de Giesen, Hans Weel and Brian du Pont for setting up and carrying out the cold rolling trials. The discussions with Michael Abspoel, Marc Scholting, Marcel Lansbergen and Hans Mulder on yield loci were greatly appreciated. This research did not receive any specific grant from funding agencies in the public, commercial, or not-for-profit sectors.

Appendix A. : Overview of all rolling experiments

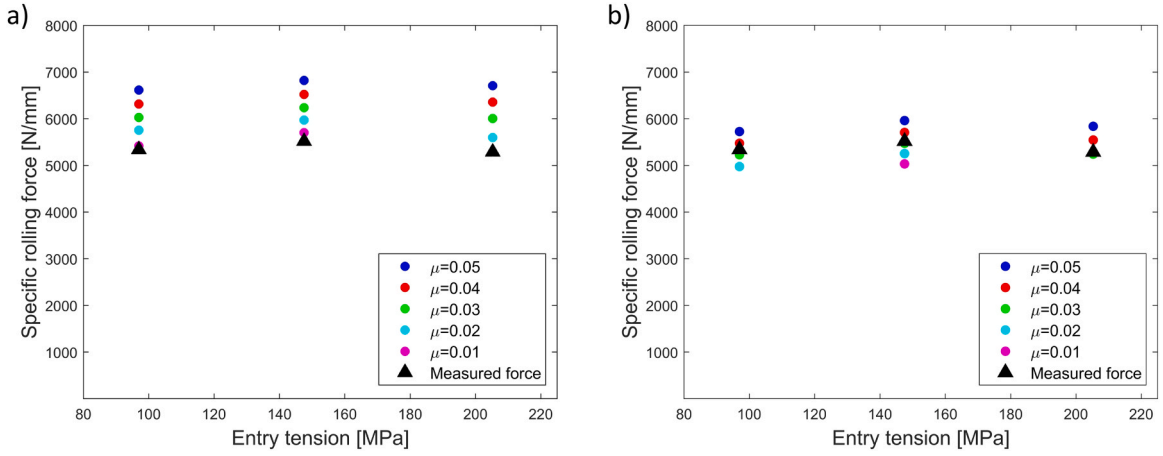

Fig. 16. Rolling force versus entry tension for pass 1 with grade A; comparison of measured values with model predictions. a) for rolling model with isotropic material yielding, b) for rolling model with anisotropic material yielding.

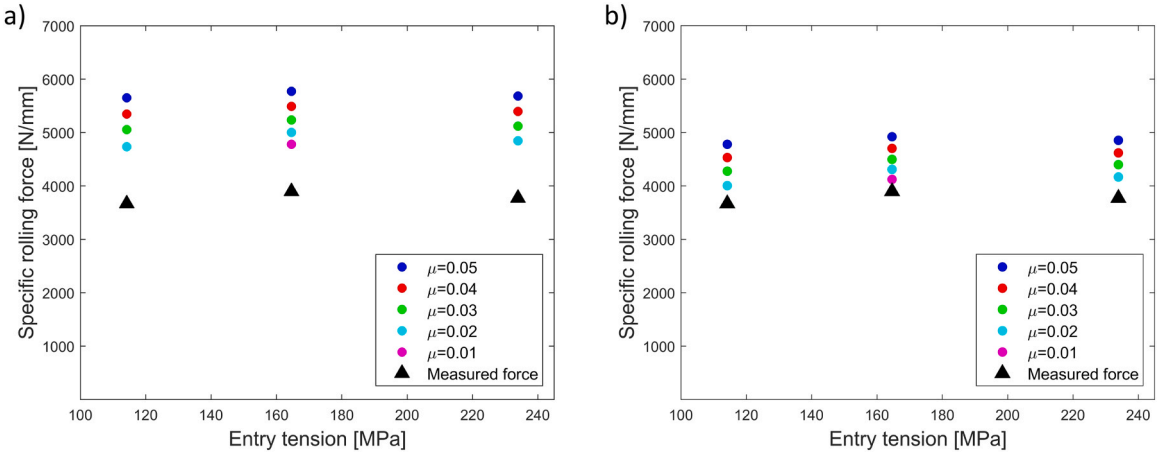

Fig. 17. Rolling force versus entry tension for pass 2 with grade A; comparison of measured values with model predictions. a) for rolling model with isotropic material yielding, b) for rolling model with anisotropic material yielding.

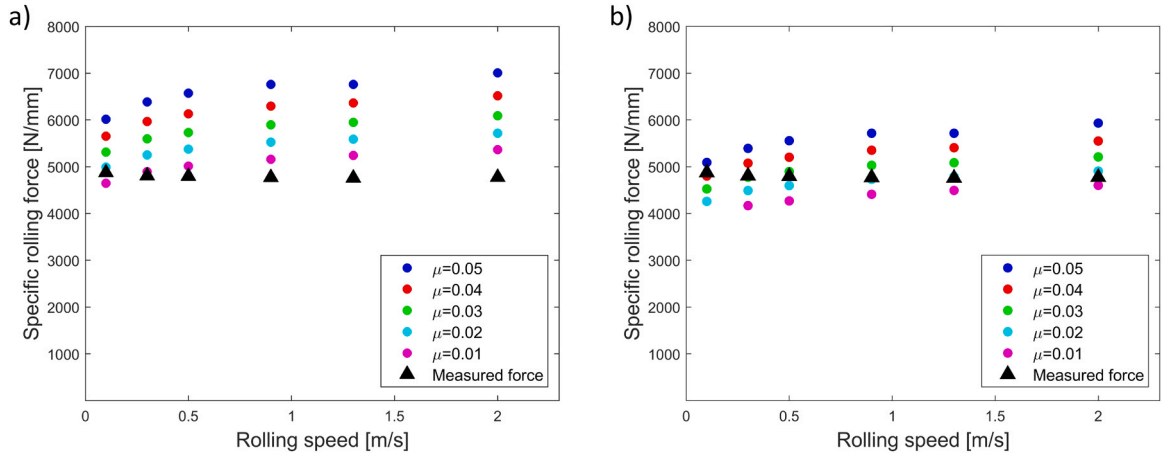

Fig. 18. Rolling force versus rolling speed for pass 3 with grade A; comparison of measured values with model predictions. a) for rolling model with isotropic material yielding, b) for rolling model with anisotropic material yielding.

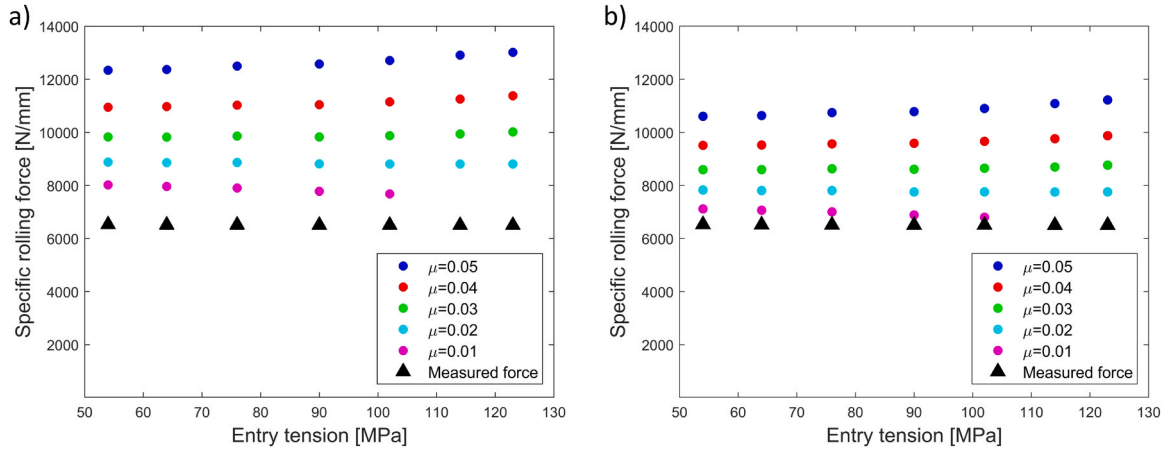

Fig. 19. Rolling force versus entry tension for pass 4 with grade A; comparison of measured values with model predictions. a) for rolling model with isotropic material yielding, b) for rolling model with anisotropic material yielding.

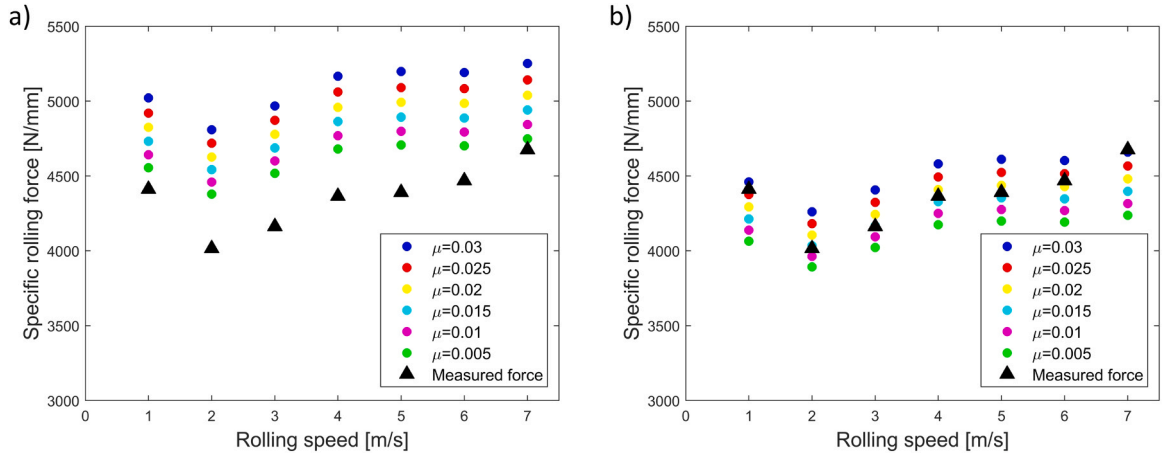

Fig. 20. Rolling force versus rolling speed for pass 1 with grade B; comparison of measured values with model predictions. a) for rolling model with isotropic material yielding, b) for rolling model with anisotropic material yielding.

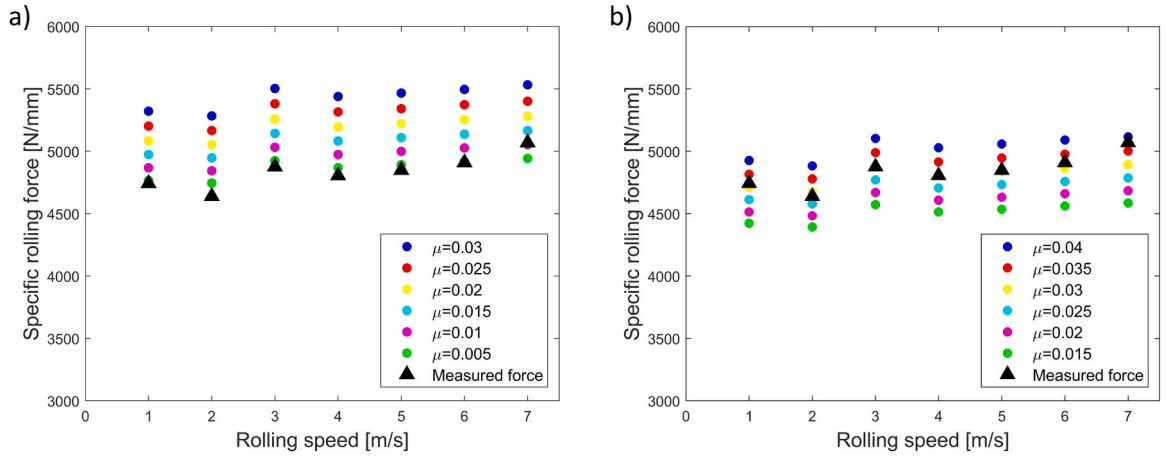

Fig. 21. Rolling force versus rolling speed for pass 2 with grade B; comparison of measured values with model predictions. a) for rolling model with isotropic material yielding, b) for rolling model with anisotropic material yielding.

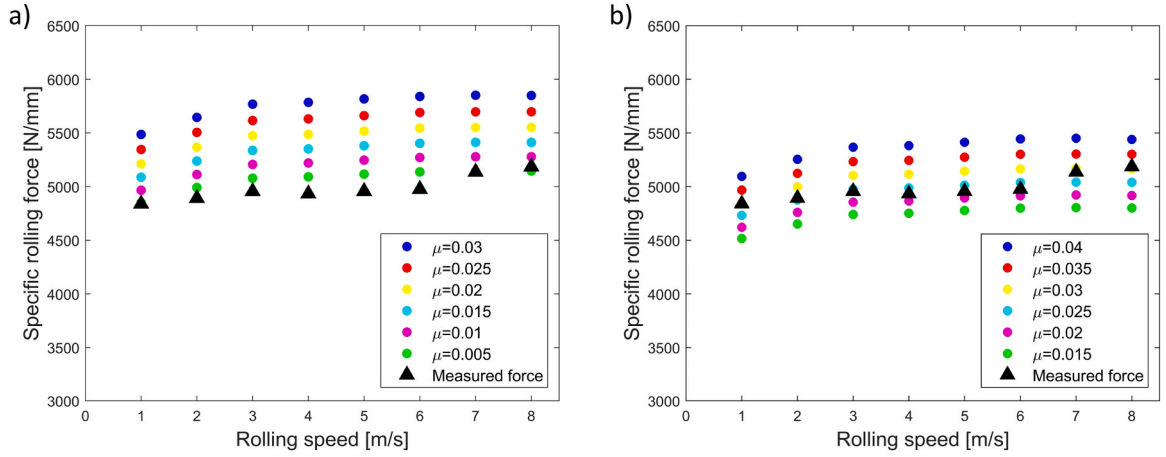

Fig. 22. Rolling force versus rolling speed for pass 3 with grade B; comparison of measured values with model predictions. a) for rolling model with isotropic material yielding, b) for rolling model with anisotropic material yielding.

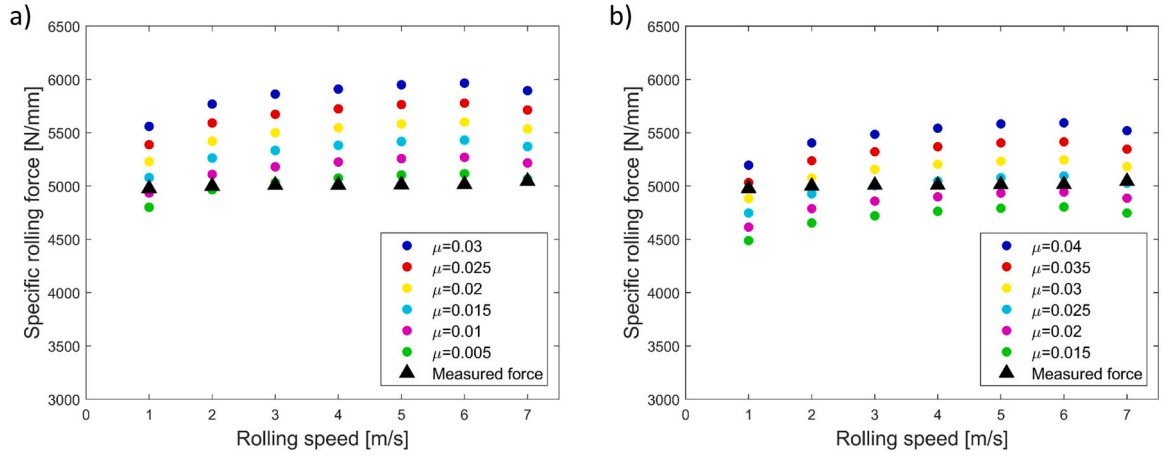

Fig. 23. Rolling force versus rolling speed for pass 4 with grade B; comparison of measured values with model predictions. a) for rolling model with isotropic material yielding, b) for rolling model with anisotropic material yielding.

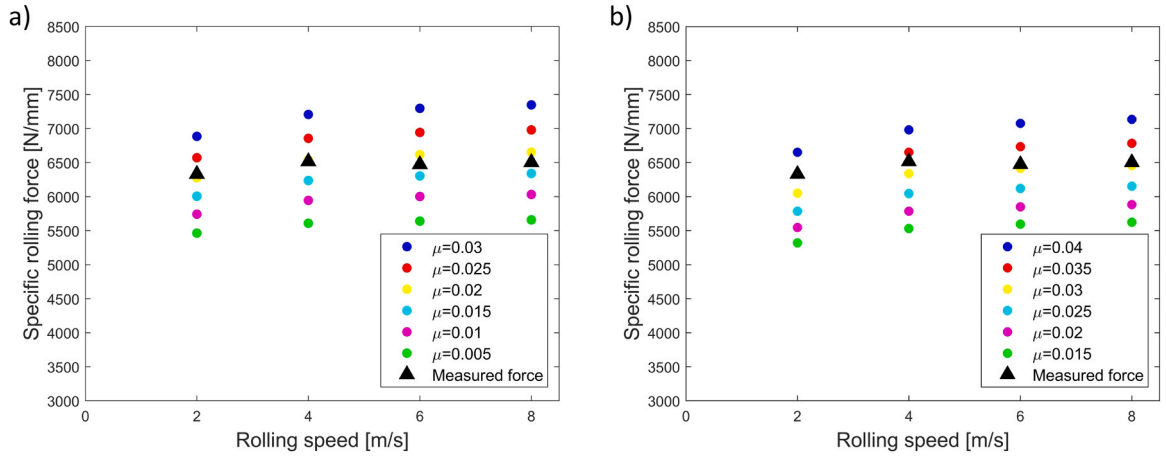

Fig. 24. Rolling force versus rolling speed for pass 5 with grade B; comparison of measured values with model predictions. a) for rolling model with isotropic material yielding, b) for rolling model with anisotropic material yielding.

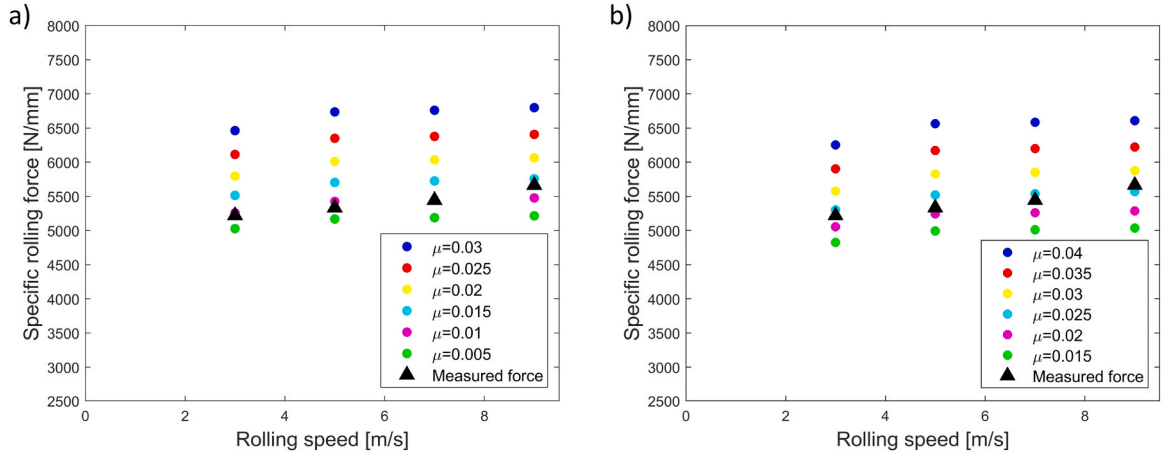

Fig. 25. Rolling force versus rolling speed for pass 6 with grade B; comparison of measured values with model predictions. a) for rolling model with isotropic material yielding, b) for rolling model with anisotropic material yielding.

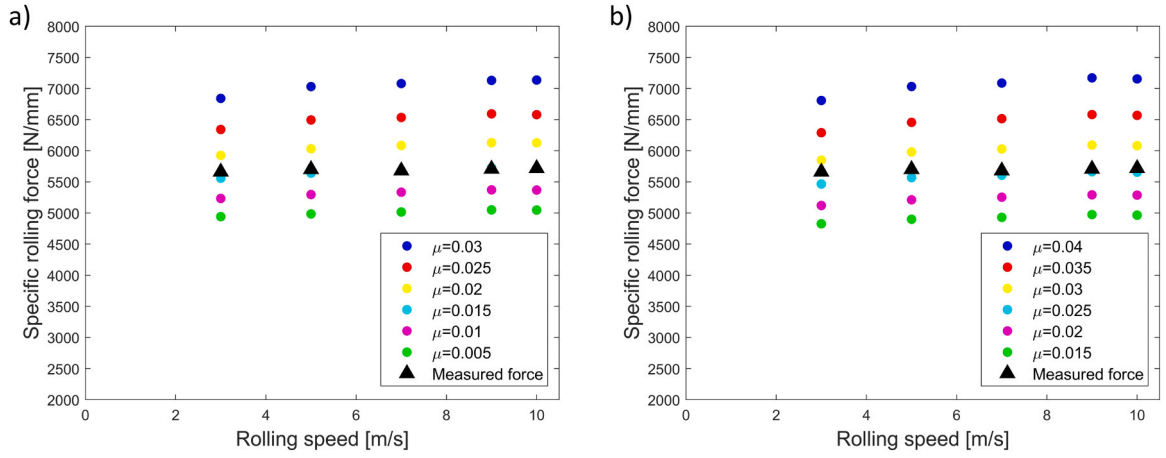

Fig. 26. Rolling force versus rolling speed for pass 7 with grade B; comparison of measured values with model predictions. a) for rolling model with isotropic material yielding, b) for rolling model with anisotropic material yielding.

In this appendix all results of the cold rolling experiments are detailed. For each rolling pass two graphs are shown, the measured rolling force is compared both with result of a cold rolling model including only isotropic material yielding as well as the same rolling model but now including anisotropic material yielding.

All graphs in the appendix support the conclusion that including anisotropic material yielding in the model results in more plausible values for the COF.

References

Abspoel M. 2022. Improved Plane Strain Prediction and Easy to Use 3D Extension for Vegter 2017 Yield Locus, *Forming Technology Forum, University of Twente*.

Abspoel, M., Scholting, M.E., Lansbergen, M., An, Y.G., Vegter, H., 2017. A new method for predicting advanced yield criteria input parameters from mechanical properties. J. Mater. Process. Technol. 248, *161–177*. https://doi.org/10.1016/j.jmatprotec.2017.05.006.

Aksenov, S.A., Kliber, J., Puzino, Y.A., Bober, S.A., 2015. Processing of plane strain compression test results for investigation of AISI-304 stainless steel constitutive behavior. J. Chem. Technol. Metall. vol. 50, *644–650*.

An, Y.G., Vegter, H., Elliott, L., 2004. A novel and simple method for the measurement of plane strain work hardening. J. Mater. Process. Technol. 155–156, 1616–1622. https://doi.org/10.1016/j.jmatprotec.2004.04.344.

Azushima, A., 2015. ISBN 978-3-319-17225-5, Chapter 3. Tribology in Sheet Rolling Technology. Springer International Publishing. https://doi.org/10.1007/978-3-319-17226-2.

Baranov, G., Ilin, K., 2022. The influence of sections on the elastic deformation of a strip on the length of the deformation zone during cold rolling. In: AIP Conference Proceedings, Vol. 2456. AIP Publishing LLC,, 020016, 10.1063/5.0074689.

Bergstrom, Y., 1969. A Dislocation Model for the Stress Strain Behaviour of Polycrystals with Special Emphasis on the Variation of the Densities of Mobile and Immobile Dislocations. Mater. Sci. Eng. Vol. 5, *193–200*. https://doi.org/10.1016/0025-5416(70)90081-9.

Boemer, D., 2020. Numerical Modeling of Friction in Lubricated Cold Rolling (PhD-thesis). University of Liège.

Brahme, A., Winning, M., Raabe, D., 2009. Prediction of cold rolling texture of steels using an artificial neural network. Comput. Mater. Sci. 46, *800–804*. https://doi.org/10.1016/j.commatsci.2009.04.014.

Bunge, H.J., 1993. Texture Analysis in Material Science: Mathematical Methods. Cuvillier Verlag, *Göttingen. ISBN 3-928815-81-4*.

Das, A., 2017. Calculation of crystallographic texture of BCC steels during cold rolling. J. Mater. Eng. Perform. 26, *2708–2720*. https://doi.org/10.1007/s11665-017-2695-6.

Deeperekha, N., Gupta, A., Demiral, M., Khatirkar, R.K., 2020. Cold rolling of an Interstitial Free (IF) Steel – experiments and simulations. Mech. Mater. 148, 103420 https://doi.org/10.1016/j.mechmat.2020.103420.

van den Boogaard A.H. 2002. Thermally Enhanced Forming of Aluminium Sheet – Modelling and Experiments*, PhD-thesis, University of Twente*.

Dorner, D., Zaefferer, S., Lahn, L., Raabe, D., 2006. Overview of microstructure and microtexture development in grain-oriented silicon steel. J. Magn. Magn. Mater. 304, *183–186*. https://doi.org/10.1016/j.jmmm.2006.02.116.

Engler, O., Huh, M.Y., Tomé, C.N., 2000. A study of through-thickness texture gradients in rolled sheets. Metall. Mater. Trans. A vol. 31A, *2299–2315*. https://doi.org/10.1007/s11661-000-0146-7.

Fouratier A., Geissler F., Endemann G. and Schmidt B. 2002. Lubrication during Cold Rolling*, EUR 20092 EN, ISBN 92–828-5191–5*.

Hill, R., 1948. A theory of the yielding and plastic flow of anisotropicmetals. Proc. R. Soc. Lond. Ser. A 193, 281–297. https://doi.org/10.1098/rspa.1948.0045.

Hitchcock J. 1935. Roll Neck Bearings*; Report of ASME Special Research Committee on Heavy-Duty Anti-Friction Bearings*.

van Houtte P. 1992. Manual of the MTM-FHM software, *Catholic University of Leuven, Belgium*.

Hutchinson, B., Artymowicz, D., 2001. Mechanisms and modelling of microstructure/texture evolution in interstitial-free steel sheets. ISIJ Int. 41, *533–541*. https://doi.org/10.2355/isijinternational.41.533.

Hutchinson, B., Ryde, L., 1997. Principles and practice of texture control in cold rolled and annealed sheet steels. 'Thermomechanical Processing in Theory, Modelling & Practice. Swedish Society for Material Technology, pp. *145–161. ISBN 9163054213*.

Inagaki, H., 1994. Fundamental aspect of texture formation in low carbon steel. ISIJ Int. 34, *313–321*. https://doi.org/10.2355/isijinternational.34.313.

Jacobs, L.J.M., van Dam, K.N.H., Wentink, D.J., de Rooij, M.B., van der Lugt, J., Schipper, D.J., Hoefnagels, J.P.M., 2022. Effect of asymmetric material entrance on lubrication in cold rolling. Tribol. Int. 175, 107810, 10.1016/j.triboint.2022.107810.

Koizumi, T., Kuroda, M., 2018. Evaluation of tension-compression asymmetry of a low-carbon steel sheet using a modified classical compression test method. J. Phys.: Conf. Ser. Vol. 1063, 012167 https://doi.org/10.1088/1742-6596/1063/1/012167.

Krabiell, A., Dahl, W., 1981. Zum Einfluss von Temperatur und Dehngeschwindigkeit auf die Streckgrenze von Baustählen unterschiedlicher Festigkeit. Arch. für Das. Eisenhüttenwes. vol. 52, *429–436*. https://doi.org/10.1002/srin.198104601.

Lange, K., 2002. Umformtechnik. Springer, Berlin, Heidelberg. *ISBN: 978-3-540-43686-7*.

Lankford, W.T., Snyder, S.C., Bauscher, J., 1950. New criteria for predicting the press performance of deep drawing sheets. Trans. ASM 42, *1197–1225*.

Li, L., Matsumoto, R., Utsunomiya, H., 2018. Experimental study of roll flattening in cold rolling process. ISIJ Int. 58, *714–720*. https://doi.org/10.2355/isijinternational.ISIJINT-2017-623.

van Liempt, P., 1994. Workhardening and substructural geometry of metals. J. Mater. Process. Technol. 45, *459–464*. https://doi.org/10.1016/0924-0136(94)90382-4.

Liu, Y.J., Tieu, A.K., Wang, D.D., Yuen, W.Y.D., 2001. Friction measurement in cold rolling. J. Mater. Process. Technol. 111, *142–145*. https://doi.org/10.1016/S0924-0136(01)00541-6.

Lucci, B.N., Lamas, W.Q., Grandinetti, F.J., Giacaglia, G.E.O., 2020. Finite element analysis applied to a metal-to-metal seal design. Braz. J. Pet. Gas. 14, *157–173*. https://doi.org/10.5419/bjpg2020-0013.

Ludwik, P., 1909. Elemente der Technologische Mechanik. Springer, Berlin.

Marzia J.A.A. 2020. Influence of the Yield Criterion in the Formability Prediction of Parts with Complex Geometry, *Master thesis University of Coimbra*. ⟨http://hdl.handle.net/10316/93932⟩.

Moerman, J., 2005. The effect of anisotropic yielding behaviour on cold rolling forces. Mater. Sci. Forum 495–497, 1517–1522. https://doi.org/10.4028/www.scientific.net/MSF.495-497.1517.

Montmitonnet, P., 2006. Hot and cold strip rolling processes. Comput. Methods Appl. Mech. Eng. 195 (48–49), 6604–6625. https://doi.org/10.1016/j.cma.2005.10.014.

Pietrzyk, M., Lenard, J.G., Dalton, G.M., 1993. A study Of The Plane Strain Compression Test. CIRP Ann. 42 (*1*), *331–334*. https://doi.org/10.1016/S0007-8506(07)62455-X.

Pires, C.T.A., Ferreira, H.C., Sales, R.M., 2009. Adaptation for tandem cold mill models. J. Mater. Process. Technol. 209, *3592–3596*. https://doi.org/10.1016/j.jmatprotec.2008.08.020.

Renavikar, M.P., Wray, P.J., Garcia, C.I., DeArdo, A.J., 2002. Role of crystallographic texture in controlling the springback behavior of ultra low carbon (ULC) steels. Iron Steelmak. (USA) 29 (*5*), *67–72*.

Schwarzer, R.A., 1991. Scanning X-ray apparatus for texture mapping by energy dispersive diffraction. Textures Microstruct. 14–18, *241–244*. https://doi.org/10.1155/TSM.14-18.241.

Shigaki, Y., Nakhoul, R., Montmitonnet, P., 2015. Numerical treatments of slipping/no-slip zones in cold rolling of thin sheets with heavy roll deformation. Lubricants 3, *113–131*. https://doi.org/10.3390/lubricants3020113.

Silk, N., van der Winden, M., 1999. Interpretation of hot plane strain compression testing of aluminium specimens. Mater. Sci. Technol. 15 (*3*), *295–300*. https://doi.org/10.1179/026708399101505860.

Spitzig, W.A., Richmond, O., 1984. The effect of pressure on the flow stress of metals. Acta Metall. 32, 457–463. https://doi.org/10.1016/0001-6160(84)90119-6.

Swift, H.W., 1952. Plastic instability under plane stress. J. Mech. Phys. Solids 1, *1–18*. https://doi.org/10.1016/0022-5096(52)90002-1.

Takajo, S., Vogel, S.C., Tomé, C.N., 2019. Viscoplastic self-consistent polycrystal modeling of texture evolution of ultra-low carbon steel during cold rolling. Modell. Simul. Mater. Sci. Eng. 27, 045003 https://doi.org/10.1088/1361–651X/ab0b92.

Tamimi, S., Gracio, J.J., Lopes, A.B., Ahzi, S., Barlat, F., 2018. Asymmetric rolling of interstitital free steel sheets: microstructural evolution and mechanical properties. J. Manuract. Process. 31, *583–592*. https://doi.org/10.1016/j.jmapro.2017.12.014.

Tresca, H., 1864. Mémoire sur l'ecoulement des corps solides soumis à de fortes pressions. Comptes Rendus De. l'Acad. Des. Sci. Paris 59, *754–758*.

Van Houtte, P., Mols, K., van Bael, A., Aernoudt, E., 1989. Application of yield loci calculated from texture data. Textures Microstruct. 11, *23–39*. https://doi.org/10.1155/TSM.11.23.

Vegter, H., van den Boogaard, A.H., 2006. A plane stress yield function for anisotropic sheet material by interpolation of biaxial stress states. Int. J. Plast. vol. 22, *499–502.*. https://doi.org/10.1016/j.ijplas.2005.04.009.

Vegter, H., Drent, P., Huétink, J., 1995. A planar isotropic yield criterion based on mechanical testing at multi-axial stress states. Proc. Fifth Int. Conf. Numer. Methods Ind. Form. Process. *345–350*.

Von Karman, T., 1925. Beitrag zur Theorie des Walzvorganges. Z. für Angew. Math. und Mech. 5, *139–141*. https://doi.org/10.1002/zamm.19250050213.

von Mises, R., 1913. Mechanik der fester Korper im plastisch-deformablen Zustand", *Nachtrichten von der Gesellschaft der Wissenschaften, Math-Phys*. Klasse *582–592*.

Wang, H., Ding, S., Taylor, T., Yanagimoto, J., 2021. Cold rolling texture prediction using finite element simulation with zooming analysis. Materials 14, *6909*. https://doi.org/10.3390/ma14226909.

Waterschoot, T., Kestens, L., de Cooman, B.C., 2002. Hot rolling texture development in CMnCrSI dual-phase steels. Metall. Mater. Trans. A 33A, *1091–1102*. https://doi.org/10.1007/s11661-002-0211-5.

Watt, D.F., Jain, M., 1984. Effec of martensite morphology on the strength differential effect in dual phase steels. Scr. Metall. 18, *1379–1382*. https://doi.org/10.1016/0036-9748(84)90369-7.

Yuen, W.Y.D., Dixon, A., Nguyen, D.N., 1996a. The modelling of the mechanics of deformation in flat rolling. J. Mater. Process. Technol. 60, *87–94*. https://doi.org/10.1016/0924-0136(96)02312-6.

Yuen, W.Y.D., Popelianski, Y., Prouten, M., 1996b. Variations of friction in the roll bite and their effects on cold strip rolling. Iron Steelmak. 23, *33–39*.

Zhou, D., Zuo, D., Wen, X., Liang, W., Yang, F., 2018. Through-thickness texture gradient and microhardness of cold-rolled AA6061. Mater. Res. Express 5, 066521. https://doi.org/10.1088/2053-1591/aac921.